




Degradation products of magnesium implant synergistically enhance bone regeneration: Unraveling the roles of hydrogen gas and alkaline environment

Yuanming An^{a,b}, Haozhi Zhang^{a,b}, Shi'an Zhang^a, Yuantao Zhang^a, Lizhen Zheng^{a,c}, Xin Chen^{a,b}, Wenxue Tong^{a,d}, Jiankun Xu^{a,d,*}, Ling Qin^{a,d,*} 

^a Musculoskeletal Research Laboratory of Department of Orthopaedics & Traumatology, Innovative Orthopaedic Biomaterial and Drug Translational Research Laboratory, Li Ka Shing Institute of Health Sciences, The Chinese University of Hong Kong, Hong Kong SAR, China

^b The Sir Yue-Kong Pao Cancer Centre, Prince of Wales Hospital, The Chinese University of Hong Kong, Hong Kong SAR, China

^c Centre for Regenerative Medicine and Health, Hong Kong Institute of Science and Innovation, Chinese Academy of Sciences, Hong Kong SAR, China

^d Centre for Musculoskeletal Degeneration and Regeneration, Department of Orthopaedics & Traumatology, Faculty of Medicine, The Chinese University of Hong Kong, Hong Kong SAR, China

ARTICLE INFO

Keywords:

Biodegradable magnesium implant
Hydrogen
Alkaline pH environment
Magnesium ions
Bone regeneration

ABSTRACT

Biodegradable magnesium (Mg) implant generally provides temporary fracture fixation and facilitates bone regeneration. However, the exact effects of generated Mg ions (Mg^{2+}), hydrogen gas (H_2), and hydroxide ions (OH^-) by Mg degradation on enhancing fracture healing are not fully understood. Here we investigate the *in vivo* degradation of Mg intramedullary nail (Mg-IMN), revealing the generation of these degradation products around the fracture site during early stages. Bulk-RNA seq indicates that H_2 and alkaline pH increase periosteal cell proliferation, while Mg^{2+} may mainly enhance extracellular matrix formation and cell adhesion in the femur *ex vivo*. *In vivo* studies further reveal that H_2 , Mg^{2+} and alkaline pH individually generate comparable effects to the enhanced bone regeneration in the Mg-IMN group. Mechanistically, the degradation products elevate sensory calcitonin gene-related peptide (CGRP) and simultaneously suppress adrenergic factors in newly formed bone. H_2 and Mg^{2+} , instead of alkaline pH, increase CGRP synthesis and inhibit adrenergic receptors. Our findings, for the first time, elucidate that Mg^{2+} , H_2 , and alkaline pH environment generated by Mg-IMN act distinctly and synergistically mediated by the skeletal interoceptive regulation to accelerate bone regeneration. These findings may advance the understanding on biological functions of Mg-IMN in fracture repair and even other bone disorders.

1. Introduction

Musculoskeletal disorders are a leading public issue worldwide, particularly osteoporotic bone fractures, which impose great burdens on the healthcare and socioeconomic systems [1,2]. Osteoporosis, a skeletal disease characterized by low bone mass and microarchitectural deterioration, affects over 200 million people worldwide, leading to heightened fracture susceptibility and increased mortality rates [3,4]. Conventional orthopaedic fixation implants, typically composed of permanent metals like stainless steel or titanium, are associated with

drawbacks such as stress shielding effects, which can hinder bone healing and often necessitate additional surgeries [5]. In recent years, magnesium (Mg) based implants have garnered attention in orthopaedic applications attributed to their superior biocompatibility, appropriate Young's modulus, and favorable osteogenic and angiogenic properties [6–9]. Our group has developed a novel Mg-containing intramedullary nail (Mg-IMN) that showed promising efficacy in enhancing fracture healing of osteoporotic bone [10], atypical femoral fractures [11], and critical bone defects [12]. However, existing studies on Mg-based implant mainly focused on the overall biological effects of pure Mg

Peer review under the responsibility of KeAi Communications Co., Ltd.

* Corresponding author. Centre for Musculoskeletal Degeneration and Regeneration, Department of Orthopaedics & Traumatology, Faculty of Medicine, The Chinese University of Hong Kong, Hong Kong SAR, China.

** Corresponding author. Centre for Musculoskeletal Degeneration and Regeneration, Department of Orthopaedics & Traumatology, Faculty of Medicine, The Chinese University of Hong Kong, Hong Kong SAR, China.

E-mail addresses: jiankunxu@cuhk.edu.hk (J. Xu), lingqin@cuhk.edu.hk (L. Qin).

<https://doi.org/10.1016/j.bioactmat.2024.12.020>

Received 26 August 2024; Received in revised form 3 December 2024; Accepted 18 December 2024

2452-199X/. 2024 The Authors. Publishing services by Elsevier B.V. on behalf of KeAi Communications Co. Ltd. This is an open access article under the CC BY-NC-ND license (<http://creativecommons.org/licenses/by-nc-nd/4.0/>).

metal or its alloys, overlooking the degradation process of Mg with byproducts Mg ions (Mg^{2+}), hydrogen gas (H_2), and hydroxide ions (OH^-) (local alkaline pH environment), through the anodic and cathodic reactions: $\text{Mg} + 2\text{H}_2\text{O} \rightarrow \text{Mg}^{2+} + 2\text{OH}^- + \text{H}_2$ [13]. The systemic investigation into the Mg implant degradation profile *in vivo* awaits to be determined.

Mg^{2+} are crucial for numerous physiological functions in human body, with approximately 60% stored in bone contributing significantly to bone formation and regeneration [14,15]. H_2 has gained attention in medical research since 2007 for its selective antioxidant properties [16], which mitigate oxidative stress and potentially aid in preventing bone loss in osteoporosis [17]. Additionally, an alkaline environment generated by OH^- has been associated with enhanced bone formation [18], countering acidic condition that typically inhibits bone growth and promotes bone resorption [19]. Despite these individual benefits, little is known about the individual or synergistic effects of Mg^{2+} , H_2 , and alkaline environment on enhanced bone regeneration by Mg-based implants.

Bone tissues are richly innervated by sensory and sympathetic nerves, which play pivotal roles in regulating bone metabolism, turnover, and fracture healing [20–22]. Sensory nerves, particularly abundant at sites of high osteogenic activity [23], produce calcitonin gene-related peptide (CGRP), a peptide known for its osteogenic effects, which were activated by Mg-IMN [10,24]. Conversely, stimulation of sympathetic neurons or sensory denervation can adversely affect bone remodeling dynamics by altering bone formation and resorption rates [25,26]. Of note, research suggested that sensory nerve activity may functionally interact with sympathetic nerve activity in bone metabolism, as the effects of sensory denervation closely resemble those of sympathetic hyperfunction [23]. Additionally, dorsal root ganglion (DRG) sensory neurons have been found to inhibit local sympathetic function in adipose tissues [27]. Despite these insights, the sympathetic regulation by Mg-based implants, and the skeletal interoceptive regulation by its degradation products have not been determined.

Given that Mg degradation releases Mg^{2+} , H_2 , and creates an alkaline environment, we hypothesize that these degradation products act distinctly but synergistically to enhance osteoporotic bone fracture healing via regulating sensory and sympathetic nerves in fracture fixation using Mg-IMN. Herein, we characterized the degradation profiles of Mg implanted in the fractured femur and explored the specific effects of its degradation products. Additionally, we *de novo* uncovered activation of sensory signals and suppression of sympathetic signals that contribute to the accelerated bone regeneration in fractured bone fixed with Mg-IMN, highlighting the comparable contributions of Mg^{2+} , H_2 , and alkaline environment in fracture healing process.

2. Materials and methods

2.1. Animals

The study utilized rats and mice from the Laboratory Animal Services Center of the Chinese University of Hong Kong. The animals were maintained in a controlled environment with a 12-h light-dark cycle and provided with unrestricted access to water and a standard rodent diet. All animal experiment procedures performed in this study adhered to the principles for the care and use of laboratory animals approved by the Animal Experimentation Ethics Committee of the Chinese University of Hong Kong (Ref. No. 22/048/MIS-5-C and 22/092/MIS-5-C). For each experiment, age-matched female animals were assigned into each group for relevant experiments randomly.

2.2. Establishment of unilaterally closed fracture model in osteoporotic rats

Female Sprague Dawley (SD) rats, aged 24 weeks, were used to establish the ovariectomy (OVX)-induced osteoporosis model and closed

femoral fracture model according to our well-established protocols [10, 11]. We designed and manufactured the strategic Mg-IMN as previously described [10]. The Mg-IMN featured eighteen interlacing holes arranged in three rows across its middle 1 cm, with an ultrapure (99.99 %) Mg cylindrical rod (ϕ 0.7 mm, length 1.5 cm) inserted into its hollow core. A traditional stainless steel intramedullary nail (SS-IMN) served as the control. The sterilized IMN was inserted vertically into the fractured femur along its axis. Post-surgery, temgesic administration at 0.05 mg/kg/day was given for three consecutive days for postoperative analgesia.

2.3. Establishment of unilaterally closed fracture model in osteoporotic mice

12-week-old female C57BL/6 mice were used to establish the standard OVX-induced osteoporosis model and closed femoral fracture model as described previously [11]. The mice were randomly assigned to three groups: Mg-IMN, SS-IMN (stainless-steel intramedullary nail), and SS-IMN + H_2 . A sterilized Mg-IMN or SS-IMN was inserted into the fractured femur along its axis. Anesthesia was provided under warm conditions, and temgesic was administered (daily and subcutaneously) for three consecutive days for postoperative analgesia. H_2 -rich water (HRW) was produced using a hydrogen water generator (NB-T71A, Shanghai Nanobubble Technology Co., Ltd., China), and tap water was always freely available as designed, hydrogen rich saline (HRS) was intraperitoneally injected for 2 weeks after fracture.

2.4. Establishment of distal femurs implantation models with IMN in rats

20-week-old female SD rats ($n = 4$ for each group) were used to establish the distal femurs implantation model. Briefly, A longitudinal incision was made at right knee and the patella was dislocated to expose the femoral condyle after anesthetized. A tunnel was created from the patella-femoral groove of the distal femur along the axis of the femoral shaft with an 18 G needle (ϕ 1.27 mm). Subsequently, the Mg-IMN, SS-IMN, $\text{Mg}(\text{OH})_2$ -IMN, MgCl_2 -IMN, and NaOH-IMN were implanted into the tunnel at the distal femur. Anesthesia was provided as written in previous paragraphs. The preparation process was as follows, we firstly sterilized salt powders and stainless-steel needles (featuring three rows of eighteen interlaced holes in the middle, identical to Mg-IMN) with ethylene oxide, placed the sterilized hollow stainless-steel needles in a centrifuge tube containing sterilized powder and continuously rolled for 12 hours to ensure thorough filling. Second, we sealed the needle tube wall with aluminum foil and placed it upright. Then, we used a fine needle to vertically squeeze the powder along the needle tube lumen, with sterilized powder continuously replenished during this process. The resulting IMNs (ϕ 0.7 mm, length 1.5 cm) were filled with compressed $\text{Mg}(\text{OH})_2$, MgCl_2 , and NaOH respectively to assembly $\text{Mg}(\text{OH})_2$ -IMN, MgCl_2 -IMN, and NaOH-IMN. All procedures were conducted in a sterilized environment with a laminar flow hood.

2.5. Microsensor measurements of H_2 and pH

Closed fractured osteoporotic rats implanted with Mg-IMN or SS-IMN from 3 days to 15 days were used for measurements of H_2 and pH value. H_2 and pH microprofiles were measured with highly sensitive microsensors and microelectrode with tip diameters of 50–100 μm on the microprofiling system (Unisense A/S, Denmark) [28]. Blood was taken from the heart to measure the H_2 concentration after heparinization with heparin (Sigma, H3393) injection at 1000 U. After exposure of the femur, H_2 was detected sequentially from the pe to central, starting with the periosteum, the surface of callus, and then within the callus. A hole in the femur was created by a 1.0 mm electric drill, and the H_2 concentration of bone marrow was measured. Subsequently, a second hole was drilled to allow both the pH microelectrode and the reference electrode were mounted on the micromanipulator, and the values were

recorded.

2.6. SEM/EDS of Mg-IMN

The thick, ground methyl methacrylate (MMA) sections were polished and sputter-coated with an approximate 10.0 nm layer of gold-palladium film for scanning electron microscope (SEM) imaging of Mg-IMN surface and energy dispersive x-ray spectroscopy (EDS) for elemental analysis using a tungsten-filament electron and low vacuum secondary electron TESCAN detector (TESCAN VEGA3, Czechoslovakia). EDS mapping analysis, EDS line analysis, and elemental composition percentage were conducted and analyzed by setting Mg, Ca, P, O, C, and Fe as the target elements for semi-quantitative measurement of their corresponding intensities. Line-scanning models were used to analyze the surface of the Mg-IMN in longitudinal and horizontal orientations. Additionally, regions of interest (ROI) near the hole and shielding region at designed time point were performed for statistical analysis.

2.7. Immunohistochemistry and histomorphometry

For bone immunohistochemistry, femora were removed from rats or mice and fixed in 4% paraformaldehyde for 3 days. The femora were decalcified in 12.5% EDTA at room temperature, then sections of 5 μ m in thickness were prepared for immunohistochemistry staining using a standard protocol. In details, the samples were deparaffinized and rehydrated, followed by the quenching of endogenous peroxidase activity using 3% hydrogen peroxide in methanol for 20min. Antigen retrieval was then achieved by treating the samples with 10 mM warm citrate buffer at 95°C for 20 minutes. Non-specific binding sites were blocked with a blocking solution containing 1 % bovine serum albumin (BSA, Thermo Fisher Scientific, USA), 5% fetal bovine serum (FBS, Thermo Fisher Scientific, USA), 0.3M Glycine, and 0.3% Triton X-100 for 1 hour. The samples were then incubated overnight at 4°C with primary antibodies against osterix (ab209484, Abcam, 1:200), Runx2 (ab192256, Abcam, 1:200), Ki67 (ab16667, Abcam, 1:200), DMP1 (PA5-120492, Thermo Fisher Scientific, USA, 1:200), CGRP (ab47027, Abcam, 1:200), SP (PA5-75165, Thermo Fisher Scientific, 1:200), NE (ab8887, Abcam, 1:600), TH (ab137869, Abcam, 1:300), ADRA1 (PA1-047, Thermo Fisher Scientific, 1:200), ADRA2 (Thermo Fisher Scientific, PA1-048, 1:200), ADRB1 (Thermo Fisher Scientific, PA5-95742, 1:200), ADRB2 (Abcam, ab182136, 1:200), ADRB3 (Abcam, ab94506, 1:200). Slides were also incubated with the blocking solution only as negative control. Subsequently, unbound primary antibodies were washed away with PBS, and the samples were incubated with the second antibody conjugated to horseradish peroxidase (Goat anti-rabbit IgG H&L HRP, Abcam, ab6721, 1:400) at room temperature for 1 hour. The DAB/HRP system (ab80436, Abcam) was then incubated for 5 minutes to detect immunoactivities, followed by counterstaining with hematoxylin. The stained sections were dehydrated, mounted and observed under light microscopy (Leica Q500MC, Leica Cambridge Ltd, Cambridge, UK).

For bone histomorphometry, femora were removed from rat or mice and fixed in 4% paraformaldehyde for 3 days. Then they were decalcified in 12.5% EDTA at room temperature, and sections with a thickness of 5 μ m were stained using hematoxylin and eosin (H&E) (H9627, and 199540 Sigma-Aldrich) and TRAP (387A, Sigma-Aldrich) according to the manufacturer's instructions. 0.05% Fast Green was used for counterstaining.

2.8. Micro-CT analysis

The Mg-IMN or SS-IMN was carefully removed from the fracture femur, then the samples were then scanned by micro-CT scanning (μ CT40, Scanco Medical, Brüttisellen, Switzerland) with resolution of 0.5 μ m/voxel as previously reported [10]. The scan range was set at 3.0 mm (286 slides), with the fracture line strategically aligned at the central point of this scanning range. And the mineralized tissue was

identified using a standardized threshold (>150 for 2 weeks post-fracture) for 3D reconstruction with a low-pass Gaussian filter (Sigma = 1.2, Support = 2).

For rat distal femur implantation samples, the implants were carefully removed before subjecting the specimens to micro-CT scanning (μ CT40, Scanco Medical, Brüttisellen, Switzerland), following regular procedures [10]. The scan range was set at 3.0 mm with 285 slides for the middle shaft analysis, with a resolution of 17.5 μ m per voxel. The mineralized bone tissue was applying a predetermined standardized intensity threshold of >165 of selected 2D images. The 3D reconstruction of the mineralized tissue was performed utilizing a low-pass Gaussian filter (Sigma = 1.2, Support = 2). Morphometric parameters included ratio of BV to TV (BV/TV), bone mineral density (BMD), ρ -moment of inertia (ρ MOI).

2.9. Enzyme-linked immunosorbent assay

The DRG taken from one side of rat were immersed in hydrogen-rich medium (HRM), alkaline pH 8.5 medium, and 10 mM Mg²⁺ medium, respectively. For the other side, the same number of DRG as the treated groups were as control group immersing in neurobasal™ plus medium (A3582901, Thermo Fisher Scientific) with the B-27™ supplement (10889038, Thermo Fisher Scientific), 20 ng/ml NGF (N2513, Sigma-Aldrich), 10^{−5} M fluorodeoxyuridine (F0503, Sigma-Aldrich), 10^{−5} M uridine (U3003, Sigma-Aldrich), 1% penicillin-streptomycin-neomycin (PSN) antibiotic mixture (15640055, Thermo Fisher Scientific), and protein stabilization (0.2% polyvinyl pyrrolidone, 0.05% sodium azide, all from Sigma-Aldrich). The culture supernatants were collected for enzyme-linked immunosorbent assay (ELISA) assay. The concentrations of CGRP and SP were detected by CGRP ELISA kit (MyBioSource, MBS727982) and SP ELISA kit (MyBioSource, MBS728320) using 100 μ l of supernatants from each specimen according to the specific ELISA kit per the manufacturer's protocol.

2.10. Sample preparation for frozen sections

The DRGs of SD rats were isolated and collected as our well-established procedure [10]. Then fixed in 4% paraformaldehyde for 24 hours, dehydrated in 30%-sucrose solution, and embedded in optimum cutting temperature (OCT, 4583, Sakura Finetek, Torrance, CA, USA) embedding medium. Cryosections with a thickness of 8 μ m were prepared by a Leica cryostat microtome for immunofluorescence staining.

2.11. Immunofluorescence

The frozen section slides were thawed at room temperature for 10 min, rehydrated with PBS, and blocked for 1 hour with 1% bovine serum albumin (BSA, Thermo Fisher Scientific, USA), 5% fetal bovine serum (FBS, Thermo Fisher Scientific, USA), 0.3M Glycine, and 0.3% Triton X-100 in PBS, followed by incubation overnight at 4°C with primary antibodies against CGRP (ab47027, Abcam, 1:150) and SP (PA5-75165, Thermo Fisher Scientific, 1:150). Then, samples were washed three times with PBS and incubated by a fluorescence-conjugated secondary antibody (ab150077, Abcam, 1:400) for 1 hour followed by washing three times with PBS. The samples were mounted with DAPI (ProLong™ gold antifade mountant with DNA stain DAPI, P36941, Thermo Fisher Scientific). Images were acquired with a fluorescence microscopy (Leica Q500MC, Leica Cambridge Ltd, Cambridge, UK).

2.12. RNA sequencing

Periosteum was isolated and scraped from femurs incubated in HRM, alkaline pH 8.5 medium, and 10 mM Mg²⁺ medium (α -MEM, 12571063, Thermo Fisher Scientific) for 24 hours at 37°C, and then enzymatically digested in α -MEM supplemented with 10% FBS and 1 mg/ml type I

collagenase (SCR103, Sigma-Aldrich) at 37°C incubator with 5% CO₂ overnight. Cells were passed through a 70 µm nylon strainer (Corning Falcon), followed by centrifugation at 1000 rpm for 5 min and lysis for RNA extraction. Callus from fractured osteoporotic rat femur at 9 days were collected. Total RNA was isolated using Trizol and PureLink RNA Mini Kit (12183018A, Life Technologies). The qualified RNA was sent to the BGI Health (HK) Company (<https://www.hkgbi.com/>) to prepare the library and sequencing. The analysis of sequencing data was performed by Dr. Tom (BGI Health, HK). Volcano maps of all significantly differentially expressed genes (DEGs), heat map of top DEGs, Gene Ontology (GO) enrichment analysis and Kyoto Encyclopedia of Genes and Genomes (KEGG) pathway enrichment were analyzed. DEGs were set as $|\log_2 \text{fold change}| > 0$ and $p < 0.05$, for each group, calluses from 4 separate rats were combined as one sample for bulk RNA sequencing.

2.13. Statistical analysis

The quantitative data from all the experiments were obtained from samples in each group. The numerical data were presented as means \pm SD. Comparisons between the two groups were analyzed using a two-tailed, unpaired Student's *t*-test. Analysis of variance (ANOVA) followed by relevant *post hoc* tests was employed when multiple groups were compared. The statistical analysis was conducted using GraphPad Prism software (Version 9.4.1, San Diego, CA, USA) software. $p < 0.05$ was considered to be statistically significant, with *n* as the number of animals. $*p < 0.05$, $**p < 0.01$, and $***p < 0.001$ were considered significant.

3. Results

3.1. Temporal-spatial degradation profiles of Mg compartment in Mg-IMN implanted in osteoporotic fracture femur in vivo

H₂ concentrations in blood and tissues around the fracture site, including the periosteum, peripheral and central callus, and bone marrow were measured. Using highly sensitive microsensors and micro electrodes (Fig. 1A), we observed H₂ signals from 3 days to 12 days post-fracture in the Mg-IMN group, while no detectable signals at day 15 (Fig. 1B). Regarding spatial distribution, the released H₂ was predominantly localized in the periosteum, peripheral callus, central callus, and bone marrow, but was absent in the circulatory blood (Fig. 1C). Elevated H₂ concentrations were particularly notable near the fracture line, peaking at 220 µmol/L in bone marrow and 40 µmol/L in callus at 3 days, followed by a second peak at 9 days (400 µmol/L in bone marrow and 40 µmol/L in callus) (Fig. 1D). Notably, no H₂ signal was detected in the non-fracture site or the contralateral side of fracture femur implanted with Mg-IMN of the same rat (Fig. 1B–E), suggesting a localized increase in H₂ levels surrounding the bone-implant interface near the fracture line within 15 days post-fracture.

We also measured pH values in the bone marrow at the fracture site. In the Mg-IMN group, pH levels mirrored those of H₂ (Fig. 1F), becoming alkaline (pH 8.5) at 3 days, buffering to 7.5 at 6 days, and peaking again at pH 8.5 at 9 days, maintaining neutrality thereafter. Conversely, the SS-IMN group showed neutral to slightly alkaline pH values (pH 7.8) at 12 days post-fracture. Bone marrow pH in the fractured femur fixed with Mg-IMN was notably alkaline (pH 8.5) at 9 days, whereas the contralateral femur remained around pH 7.4 (Fig. 1G), indicating an alkaline environment localized near the tissues around the implant but not affecting bulk pH (the overall acidity or alkalinity of liquid).

Initially, a highly pure Mg metal rod (99.99% purity) was inserted into the hollow intramedullary needle. Scanning electron microscopy (SEM) revealed Mg degradation during the early phase of fracture healing, with Mg elements diffusing into the hole region of IMN (Fig. 1H). Elemental composition percentages analysis showed Mg content in the hole region increased significantly to 20% at 9 and 15 days post-fracture, stabilizing around 3% at 6 weeks and 12 weeks

(Fig. 1I), indicating a significant increase of Mg during the early stage but an obvious decrease in the later stages of fracture healing.

Collectively, these data demonstrate that Mg metal degrades upon implantation in the fractured femur, leading to localized H₂ generation, alkaline pH environment, and elevated Mg²⁺ level during the early stage of osteoporotic fracture healing.

3.2. Individual biological effects of three Mg degradation products on femur ex vivo

The direct effects of H₂, alkaline pH environment, and Mg²⁺ on bone regeneration were investigated *ex vivo*. The periosteum comprises outer fibrous and inner cambium layers which rich in mesenchymal and osteogenic progenitors [29]. Histological analysis of isolated rat femur treated with saturated H₂ rich medium (HRM), alkaline pH 8.5 medium, and 10 mM Mg²⁺ medium for 24 hours showed that H₂ and alkaline pH treatment led to a thicker inner osteogenic layer in rat femur (Fig. 2A). Both H₂ and alkaline pH treatment increased the expression of Ki67, a proliferation marker [30], in the periosteum osteogenic layer. Mg²⁺ treatment did not significantly increase the Ki67 expression (Fig. 2A). Additionally, all the treatments enhanced the expression of Runx2 and DMP1 (Fig. 2A), which are crucial for osteoblastic differentiation [31] and osteocytes function [32], indicating their potential influence on bone regeneration and osteogenesis *ex vivo*.

To further explore the mechanisms underlying the effects of these degradation products on bone regeneration, RNA-Seq analysis was conducted on periosteum isolated from rat femur immersed in HRW, alkaline pH 8.5, and 10 mM Mg²⁺ medium for 24 hours *ex vivo*. The analysis revealed significant differentially expressed genes (DEGs): 1489 up-regulated and 1470 down-regulated DEGs with HRW treatment, 2641 up-regulated and 2921 down-regulated DEGs with pH 8.5 treatment, and 440 up-regulated and 452 down-regulated DEGs with 10 mM Mg²⁺ treatment (Fig. 2B). Pathways analysis using Kyoto Encyclopedia of Genes and Genomes (KEGG) highlighted enrichment in pathways related to pluripotency of stem cells, mTOR signaling pathway, TGF-β signaling pathway, and hippo signaling pathway, as well as cell fundamental cellular functions like ribosome biogenesis and protein processing, which were up-regulated by both H₂ and alkaline pH treatments. Mg²⁺ treatment up-regulated pathways involved in ECM-receptor interaction, protein digestion and absorption, and focal adhesion pathways (Fig. 2C). Furthermore, downregulated DEGs by all treatments were associated with inflammation, immunity, and apoptosis-related pathways (Fig. 2D). These findings suggest that three degradation products from Mg exert distinct and potentially synergistic effects on the gene modulation in the periosteum of femur *ex vivo* without systemic neuro regulation. Specifically, H₂ and alkaline pH might mainly enhance pathways related to pluripotency of stem cells regulation, whereas Mg²⁺ might promotes pathways involved in ECM interactions and focal adhesion by RNA-seq analysis. However, this still needs further verification.

3.3. Contribution of the degradation products from Mg-IMN to the enhanced bone regeneration in vivo

Further the individual and combined effects of Mg degradation products on bone regeneration were investigated *in vivo*. Firstly, H₂ supplementation through intraperitoneal injection of H₂-rich saline (HRS) and drinking H₂-rich water (HRW), commonly used methods of H₂ administrations [33], accelerated osteoporotic fracture healing. Both Mg-IMN and SS-IMN + HRW groups exhibited decreased fibrous tissue formation, increased cartilage and calcified new bone formation, and reduced TRAP positive cells indicating less bone resorption (Fig. 3A). Micro-CT analysis further revealed higher bone volume (BV)/tissue volume (TV) ratio and increased bone mineral density (BMD) in these groups compared to the SS-IMN group at 2 weeks (Fig. 3B), suggesting beneficial role of H₂ in early-stage healing of osteoporotic fractures in

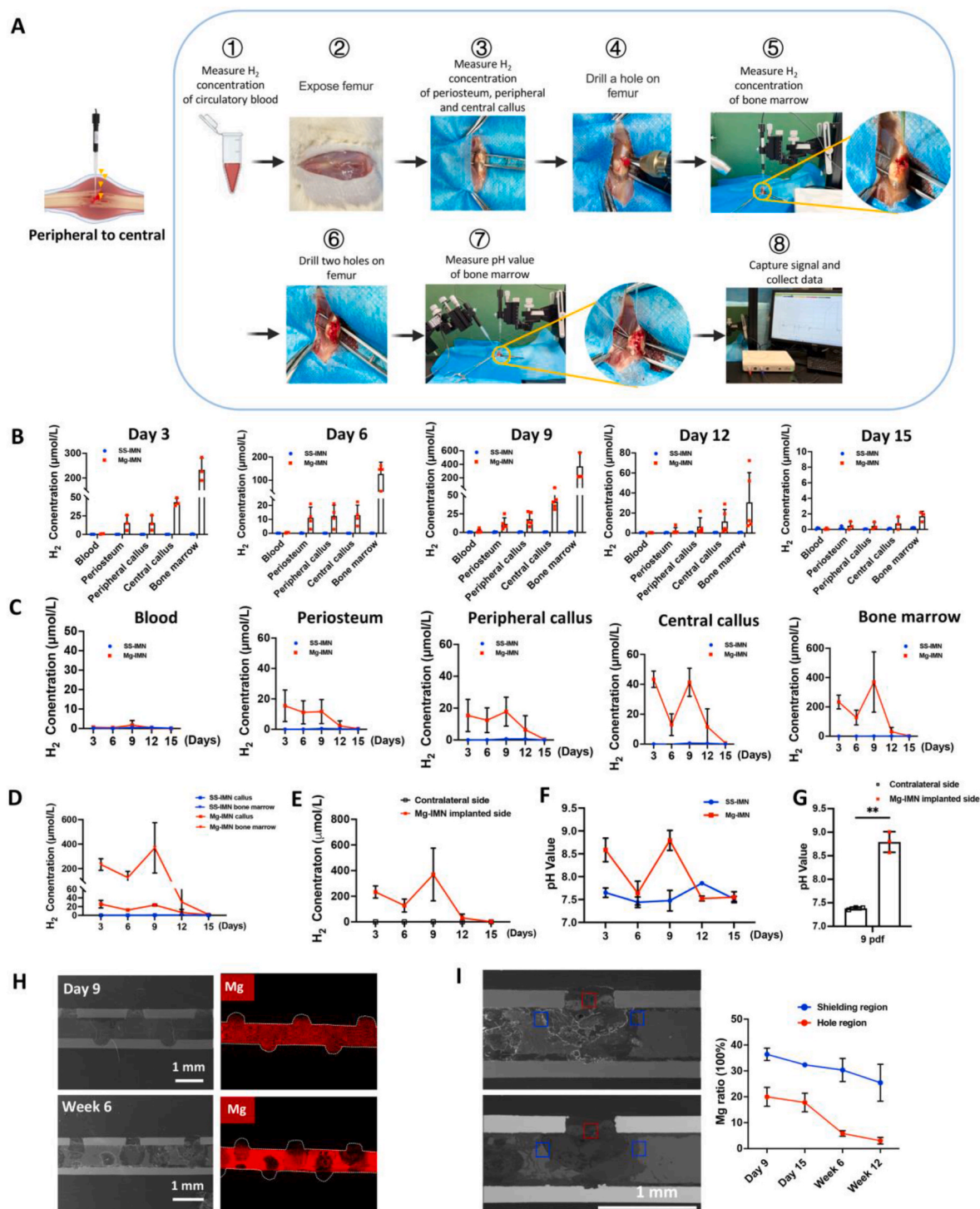
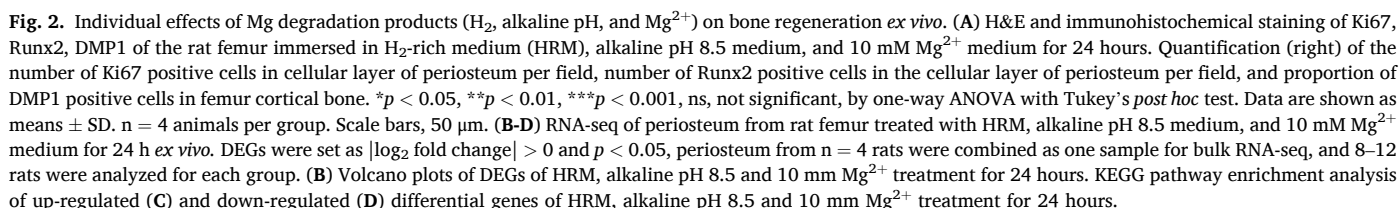


Fig. 1. Temporal-spatial degradation profiles of Mg-IMN implanted in osteoporotic fracture femur *in vivo*. (A) Schematic illustration of H_2 and pH value detection procedures in circular blood and tissues. H_2 concentration at 3 days, 6 days, 9 days, 12 days, and 15 days post-fracture (B) of blood and tissues surrounding the fracture gap including periosteum, peripheral callus, central callus and bone marrow (C) of fractured osteoporotic rat femur implanted with Mg-IMN and SS-IMN. $n = 3$ –5 rats per group. H_2 concentration of callus (average value of the periosteum, peripheral callus and central callus) and bone marrow of the fractured femur (D) implanted with Mg-IMN or SS-IMN, and contralateral femur (E) at 3 days, 6 days, 9 days, 12 days, and 15 days post-fracture. $n = 3$ –5 rats per group. pH value of bone marrow of fractured rat femur implanted with Mg-IMN or SS-IMN at 3 days, 6 days, 9 days, 12 days, and 15 days post-fracture (F) and the pH value of Mg-IMN implanted fractured femur and its contralateral femur at 9 days post-fracture (G). Data are shown as means \pm SD. $n = 3$ for each group. **, $p < 0.01$, significant difference of Mg-IMN implanted side from the contralateral side of the same rat. (H) EDS analysis of Mg-IMN at 9 days and 6 weeks. Scale bar, 1.0 mm. Lining EDS analysis and chemical composition determination of Mg-IMN at 6 weeks. Scale bar, 1 mm. (I) Elemental composition percentage of Mg-IMN in the hole (red rectangle) and the shielding region (blue rectangle) from 9 days, 15 days, 6 weeks, and 12 weeks post-Mg-IMN implantation in the fractured femur. $n = 7$ –11 regions of interests (ROIs) for each group per time point.



Considering the potential systemic effects of intraperitoneal HRS injection and oral HRW drinking, we eliminated H₂ effects to focus on the specific impacts of Mg degradation products. Compressed salt-containing IMN including Mg(OH)₂-IMN, MgCl₂-IMN, and NaOH-IMN, as well as SS-IMN and Mg-IMN were implanted in rat distal femurs. Micro-CT measurements confirmed the osteogenic effects across all

treated groups, with significantly increased total bone volume (TV), highly mineralized bone volume (BV), and polar moment of inertia (ρ MOI) compared to controls (Fig. 3C). Differences were observed in the newly formed bone at the peripheral cortex due to the separate or combined treatments with degradation products (Fig. 3D). Notably, Mg-IMN led to substantial new bone formation in the peripheral cortex of distal femurs, whereas $\text{Mg}(\text{OH})_2$ -IMN, MgCl_2 -IMN, and NaOH-IMN

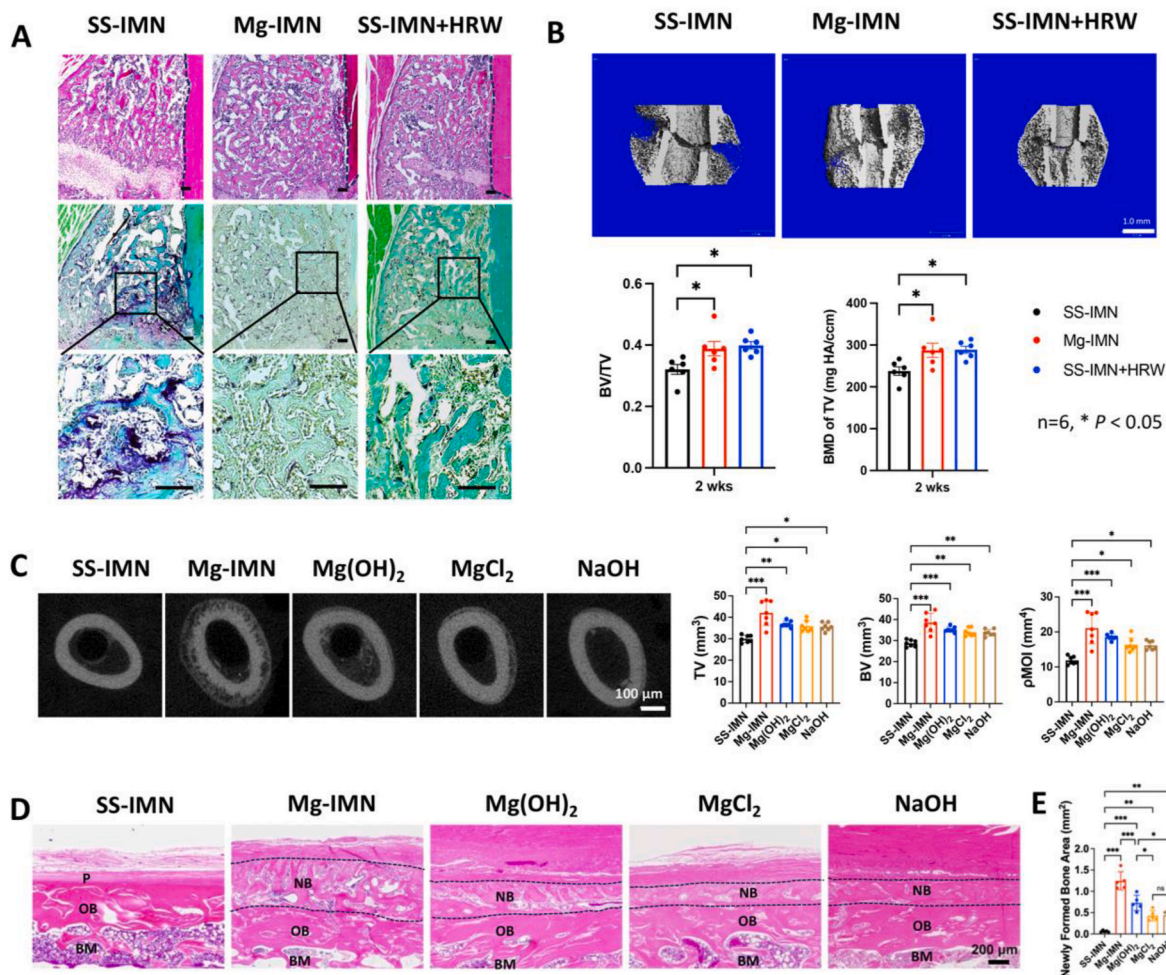


Fig. 3. The contribution of the degradation products from Mg-IMN to enhanced bone regeneration. (A) Representative H&E and TRAP staining of the osteoporotic fracture callus at 2 weeks in SS-IMN group, Mg-IMN group, and SS-IMN + H₂-rich water (HRW) group. Scale bars, 100 μ m. (B) Representative micro-CT images and measurements (below) of BV/TV, BMD of the osteoporotic fracture callus at 2 weeks in SS-IMN group, Mg-IMN group, and SS-IMN + HRW group. * p < 0.05, by one-way ANOVA with Tukey's *post hoc* test. Data are shown as means \pm SD. n = 6 animals per group. Scale bar, 1.0 mm. (C) Representative micro-CT images and measurements (right) of BV, TV, pMOI of the newly formed bone at the peripheral cortex of rat femur implanted with SS-IMN, Mg-IMN, Mg(OH)₂-IMN, MgCl₂-IMN, NaOH-IMN in the distal femur for 2 weeks. * p < 0.05, ** p < 0.01, *** p < 0.001, by one-way ANOVA with Tukey's *post hoc* test. Data are means \pm SD. n = 7 animals per group. Scale bar, 100 μ m. Representative H&E staining (D) and measurements of the newly formed bone area (E) at the peripheral cortex of rat femur implanted with SS-IMN, Mg-IMN, Mg(OH)₂-IMN, MgCl₂-IMN, NaOH-IMN in the distal femur for 2 weeks. P, periosteum. NB, newly formed bone. OB, old bone. BM, bone marrow. Scale bar, 200 μ m * p < 0.05, ** p < 0.01, *** p < 0.001, by one-way ANOVA with Tukey's *post hoc* test. Data are means \pm SD. n = 5 animals per group.

showed smaller area of newly formed bone compared to Mg-IMN (Fig. 3E), highlighting the significant role of all three degradation products in promoting bone formation.

3.4. Mg-IMN accelerated the early stage of fracture healing process in osteoporotic bone through inhibiting adrenergic signaling

The effect of Mg-IMN during the early healing process (3 days, 6 days, 9 days, 12 days, 15 days post-fracture) of osteoporotic fracture was explored. The Mg-IMN group showed significant granulation tissue accumulation at 3 days, whereas the SS-IMN group exhibited fragmented bone with minimal granulation tissue (Fig. 4A). By day 6, larger cartilage formations and numerous foci of immature woven trabecular bone were evident in the Mg-IMN group compared to the SS-IMN group. From 9 to 15 days, the Mg-IMN implantation displayed increased callus maturation with more mature osteoid matrix, trabecular bone-like structures, and bony callus replacement, with early signs of remodeling observed as lamellar bones dispersed among woven bones (Fig. 4A). In contrast, similar maturation and remodeling processes were delayed in the SS-IMN group, becoming noticeable around 15 days (Fig. 4A).

TRAP staining at 15 days confirmed more osteoclast activity in the callus of the Mg-IMN group compared to SS-IMN (Fig. 4B). Immunohistochemistry further revealed upregulated expression of Sp7 (Osterix) and Runx2, markers crucial for osteogenesis, in the Mg-IMN group at 9 days (Fig. 4C), suggesting accelerated osteogenesis by Mg-IMN approximately 3 days earlier than SS-IMN. Additionally, small voids observed in the soft callus at 3 days gradually diminished by 15 days, indicating gas production possibly accompanied by diffusion into surrounding tissues. These findings collectively demonstrate that Mg-IMN implantation accelerates the early regeneration process of osteoporotic fractures, facilitated by H₂ production and diffusion around the fracture site.

The potential regulatory mechanism underlying the accelerated early phase of the bone fracture regeneration process by Mg-IMN was further explored through bulk-RNA sequencing analysis of rat callus. The degradation profile revealed peak H₂ concentration and pH values surrounding the fracture site at 9 days, concurrent with the upregulation of osteogenesis markers Osterix (Sp7) and Runx2 following Mg-IMN implantation (Fig. 4C). Therefore, the callus tissues at 9 days post-fracture were processed for RNA sequencing. The volcano plot depicted a dominant effect of Mg-IMN, whereby 1552 DEGs were up-regulated and

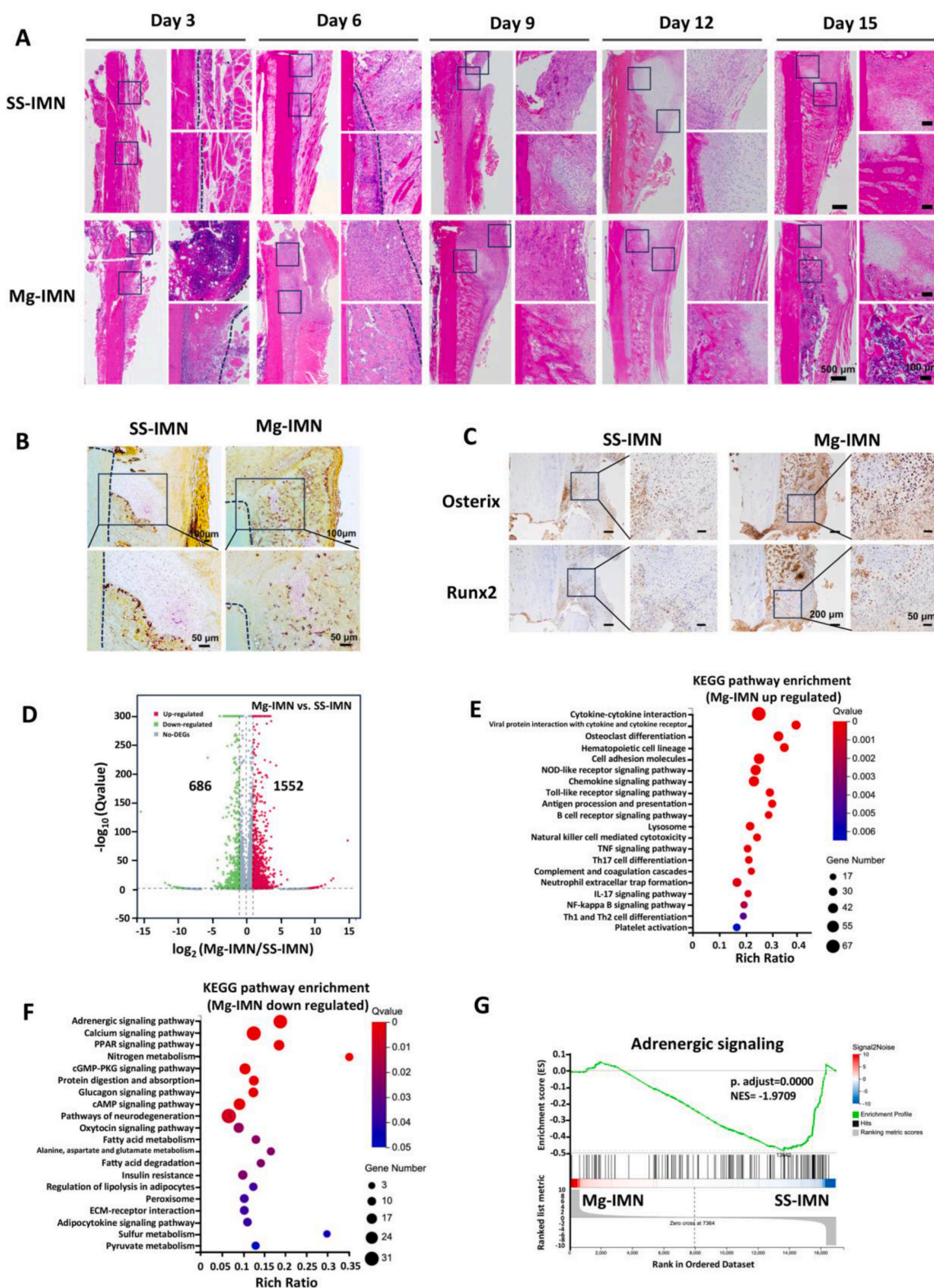


Fig. 4. Mg-IMN accelerated the early stage of osteoporotic bone fracture healing through adrenergic signaling. (A) Representative H&E staining of fractured osteoporotic rat femurs implanted with Mg-IMN or SS-IMN at 3 days, 6 days, 9 days, 12 days, and 15 days post-fracture. Scale bars, 500 μ m (main images), 100 μ m (magnified images). The residual samples were harvested from those after H₂ and pH value detection. (B) Representative TRAP staining images of the callus at 15 days treated with Mg-IMN or SS-IMN. Scale bars, 100 μ m (main images), 50 μ m (magnified images). (C) Representative immunohistochemical staining of Osterix (Sp7) and Runx2 at the fracture healing callus at 9 days post-fracture implanted with Mg-IMN or SS-IMN. Scale bars, 200 μ m (main images), 50 μ m (magnified images). (D–G) RNA-seq of the fractured femur callus of rats implanted with Mg-IMN or SS-IMN at 9 days post-fracture. DEGs were set as $|\log_2$ fold change| > 0 and p < 0.05, 4 separate callus were combined for RNA sequencing. Volcano plots of DEGs (D), Kyoto Encyclopedia of Genes and Genomes (KEGG) pathway enrichment analysis of up-regulated DEGs (E), KEGG pathway enrichment analysis of down-regulated DEGs (F), and gene set enrichment analysis (GSEA) of the adrenergic signaling pathway (G) between Mg-IMN and SS-IMN groups.

686 down-regulated (Fig. 4D). KEGG analysis of Mg-IMN up-regulated genes revealed highlighted significant enrichment of terms related to cytokine-cytokine interaction, osteoclast differentiation, hematopoietic cell lineage, and cell adhesion signaling pathways (Fig. 4E). Besides, immune responses involving toll-like receptor signaling, B cell receptor signaling, neutrophil extracellular trap formation, IL-17 signaling, Th1 and Th2 cell differentiation. were also enriched. Among the top five enriched signaling terms, Cxcl6, Ccl6, Pf4, Itgam, Itgb2, Tnn, Fgf7, Fgfr1, Col1a1, Col12a1, BMP2, BMP4, and BMP7 were sorted out. Notably, adrenergic signaling pathway emerged as the most significant enriched term by KEGG analysis of Mg-IMN down-regulated genes (Fig. 4F). Gene set enrichment analysis (GSEA), 140 adrenergic-dependent genes were used as a gene set, confirmed a strong enrichment of adrenergic-dependent genes amongst those negatively regulated by Mg-IMN, with a normalized enrichment score (NES) of -1.9709 and adjusted p-value of 0.000 (Fig. 4G). In addition, the gene expression of *Ppp1r1a*, *Ryr2*, *Adra1a*, *Scn4b*, *Cacng5*, related to adrenergic signaling were downregulated by Mg-IMN, which are the possible targets for the regulation of adrenergic signaling.

These findings suggest that Mg-IMN enhanced osteoporotic bone

regeneration during the early stage of osteoporotic bone fracture healing by potentially suppression the adrenergic signaling pathway.

3.5. Sensory and sympathetic regulation by Mg-IMN on bone fracture healing

Sensory and sympathetic nerves play critical roles in regulating bone regeneration and fracture healing [34]. Calcitonin gene-related peptide (CGRP) is the preeminent osteogenic peptide and Mg-IMN implantation induces CGRP release and accelerates bone healing [10]. The sensory and sympathetic regulation on bone regulation was further verified by immunohistochemistry analysis. Results revealed significantly increased CGRP expression in tissues surrounding the fracture sites and in osteoblasts forming calcified callus, particularly at early post-fracture stages. In contrast, implants with SS-IMN showed much lower CGRP expression (Fig. 5A). Furthermore, Mg-IMN treatment suppressed the expression of noradrenaline (NE), a key neurotransmitter of the sympathetic nervous system playing a contrasting role to CGRP in bone metabolism [20], in fibrous tissues, cartilage, and newly formed bony callus, contrasting with high NE levels observed in SS-IMN (Fig. 5B). This suppression was

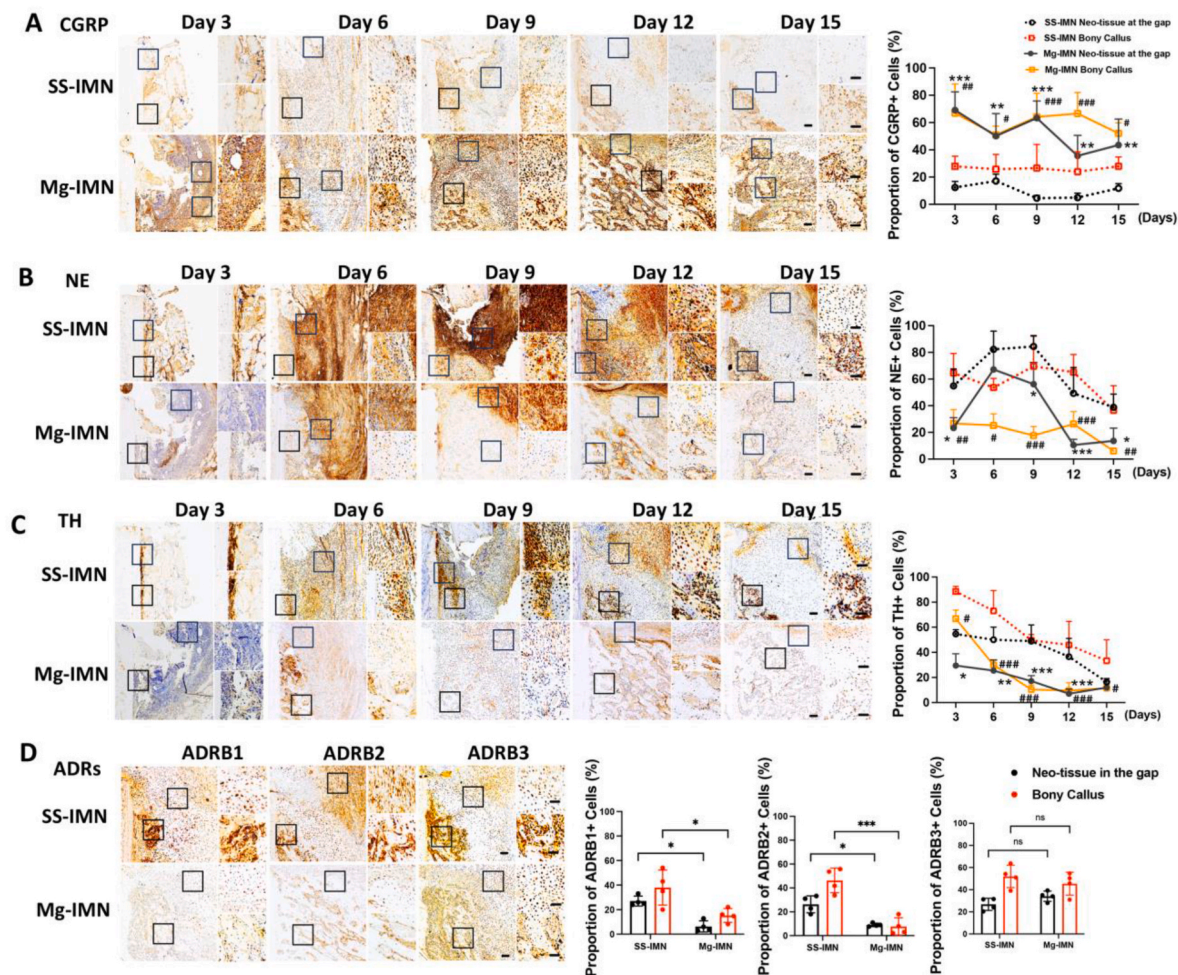


Fig. 5. Sensory and sympathetic regulation by Mg-IMN on bone regeneration. Immunohistochemical staining of CGRP (A), NE (B), and TH (C) in the neo-tissue at the fracture gap and bony-callus during the early stage of osteoporotic fracture healing implanted with Mg-IMN or SS-IMN at 3 days, 6 days, 9 days, 12 days and 15 days post fracture. Quantification (right) of the proportion of CGRP, NE and TH positive cells in neo-tissue in the gap and bony callus. Two-way ANOVA with Tukey's *post hoc* test, * $p < 0.05$, ** $p < 0.01$, *** $p < 0.001$, Mg-IMN neo-tissue in the gap vs. SS-IMN neo-tissue in the gap. # $p < 0.05$, ## $p < 0.01$, ### $p < 0.001$, Mg-IMN bony callus vs. SS-IMN bony callus. (D) Immunohistochemical staining of adrenergic receptors in the neo-tissue at the fracture gap and bony-callus during the early stage of osteoporotic fracture healing implanted with Mg-IMN or SS-IMN at 12 days post fracture. Quantification (right) of the proportion of ADRB1, ADRB2, ADRB3 positive cells in neo-tissue in the gap and bony callus. * $p < 0.05$, ** $p < 0.01$, *** $p < 0.001$, ns, not significant, by one-way ANOVA with Tukey's *post hoc* test. Data throughout are presented as means \pm SD. $n = 3$ –4 animals per group. Scale bars, 100 μ m (main images), 50 μ m (magnified images). The residual samples were harvested from those after H_2 and pH value detection.

accompanied by reduced levels of tyrosine hydroxylase (TH), the rate-limiting enzyme in catecholamine synthesis which is abundantly expressed in the sympathetic nerve fibers within the bone [20] (Fig. 5C, Fig.S1, S2). Mg-IMN also downregulated adrenergic receptors, particularly ADRB1, ADRB2 in neo-tissues surrounding the fracture gap and bony callus at 12 days post-fracture (Fig. 5D), suggesting a potential modulatory of sympathetic nervous system during bone healing.

Collectively, Mg-IMN accelerated the early bone fracture healing process, possibly through simultaneous activation of sensory CGRP pathways and suppression of sympathetic signaling.

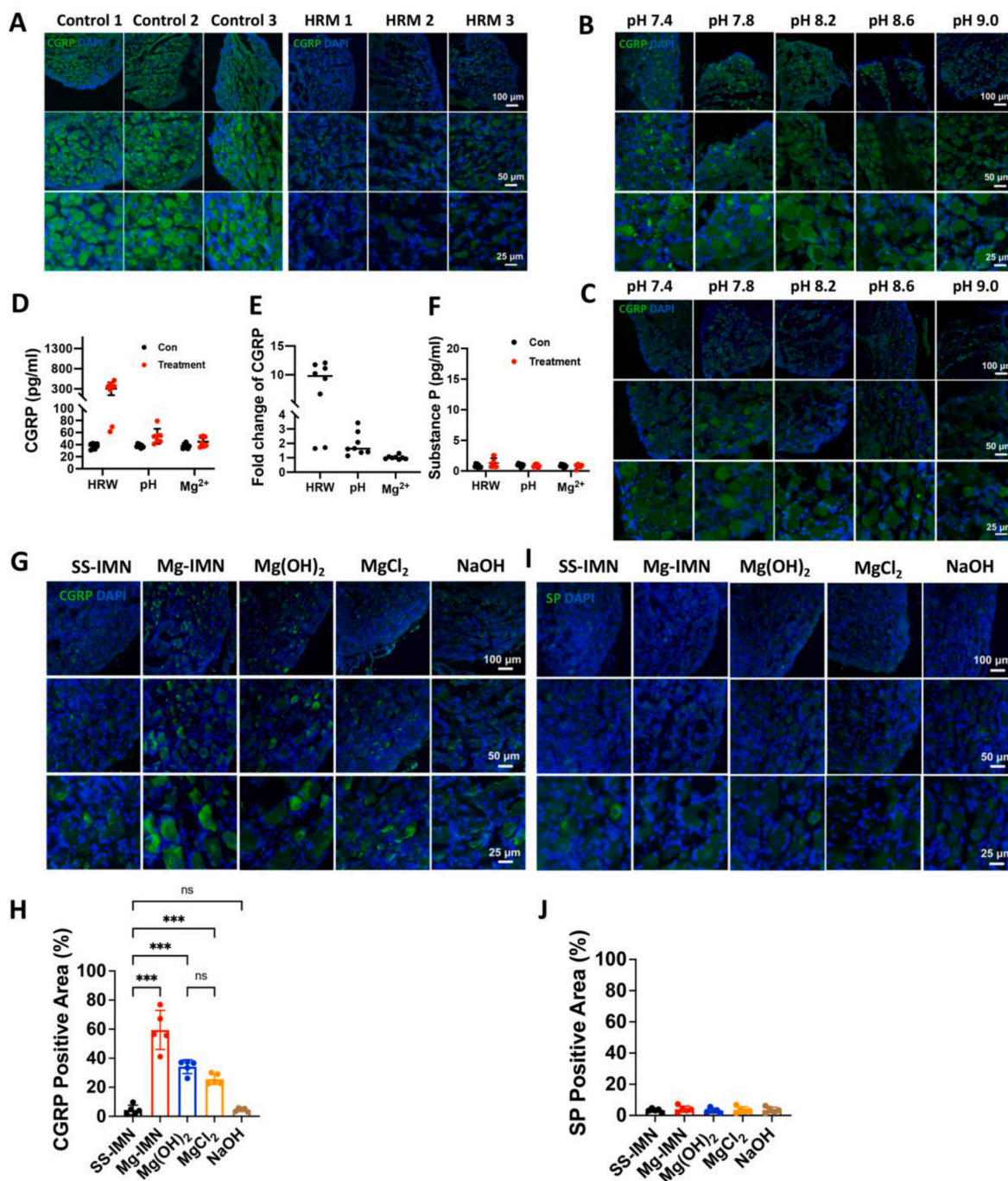


Fig. 6. Effects of the degradation products on CGRP in DRG *ex vivo* and *in vivo*. (A) Immunofluorescence staining of CGRP in DRG immersed in HRM for 2 hours. Immunofluorescence staining of CGRP expression in rat DRG immersed in alkaline pH 8.5 medium for 1 hour (B), and 2 hours (C). (D) CGRP content in the culture supernatant of medium treated with HRM, alkaline pH 8.5, and 10 mM Mg²⁺ for 2 hours *ex vivo* and untreated DRG groups *ex vivo*. (E) Fold change in CGRP levels in the culture supernatant between the same number DRGs of treated and untreated samples from the same rat, and (F) SP content in the culture supernatant of treated and untreated DRG. Data are shown as means \pm SD, $n = 8$ for each group. Immunofluorescence staining of CGRP (G), SP (I), and analysis for the proportion of CGRP positive area (H) and SP positive area (J) in T3-T5 DRG from rat implanted with SS-IMN, Mg-IMN, Mg(OH)₂-IMN, MgCl₂-IMN, or NaOH-IMN in the distal femur for 2 weeks. * $p < 0.05$, ** $p < 0.01$, *** $p < 0.001$, ns, not significant, by one-way ANOVA with Tukey's *post hoc* test, $n = 5$ animals per group. Scale bars, 100 μ m (main images), 50 μ m and 25 μ m (magnified images). Data are presented as means \pm SD.

3.6. Effects of Mg degradation products on CGRP in DRG *ex vivo* and *in vivo*

Mg-IMN implantation stimulates CGRP release from the local sensory fibers and in turn induces osteogenesis [10]. We investigated how the three degradation products of Mg-IMN influence CGRP in DRG *ex vivo* and *in vivo*. It was observed that immersion of isolated DRG in H₂ rich medium (HRM) for 2 hours significantly reduced CGRP expression in DRG (Fig. 6A). Similarly, when DRG was exposed to increasingly alkaline environments (pH 7.4 to 9.0) for 1 hour (Fig. 6B) and 2 hours (Fig. 6C), CGRP expression gradually decreased. These results suggest that both H₂ and alkaline pH environment stimulate the release of CGRP from the DRG in a relatively short period. This was further confirmed by measuring the CGRP and substance P (SP) content in the culture supernatant of rat DRG treated with HRM, alkaline pH 8.5, and 10 mM Mg²⁺ for 2 hours by ELISA analysis. HRM treatment markedly increased CGRP levels in culture supernatant to about 300 pg/ml, and pH 8.5 treatment resulted in CGRP levels of 60 pg/ml. However, Mg²⁺ treatment for 2 hours had no significant effect on CGRP release from DRG in short-time *ex vivo*, without engaging systemic nerves regulation (Fig. 6D). We also compared CGRP content in equal numbers of DRGs from the same rat, using one side for treatment and the other side as a control, confirming that CGRP (treated DRGs vs. untreated DRGs) levels increased about 10-fold with HRW treatment and 2- to 4-fold with alkaline pH 8.5 treatment. Again, Mg²⁺ treatment had little effect at 2 hours (Fig. 6E). Notably, SP levels remained unchanged by these treatments (Fig. 6F), indicating specificity in the modulation of CGRP release pathways.

Herein, *in vivo* study of degradation products on CGRP in DRG was performed via SS-IMN, Mg-IMN, Mg(OH)₂-IMN, MgCl₂-IMN, and NaOH-IMN implantation into the distal femur of rats, respectively. Immunofluorescence of L3-L5 DRG from rats implanted with Mg-IMN, Mg(OH)₂-IMN, MgCl₂-IMN, in the distal femur showed a significant increase in CGRP synthesis and synaptic vesicles accumulation (Fig. 6G and H). Conversely, SP levels remained unaffected across all groups (Fig. 6I and J). Notably, treatment with Mg²⁺, including Mg(OH)₂-IMN, and MgCl₂-IMN, led to a moderate increase in CGRP synaptic vesicles whereas the alkaline pH environment alone had little effect on CGRP synthesis (Fig. 6H). These results suggest that the enhanced CGRP synthesis in DRG induced by Mg-IMN primarily arises from Mg²⁺ and H₂, rather than from alkaline pH environment alone.

3.7. Local sensory and sympathetic regulation by Mg degradation products on bone regeneration *in vivo*

The regulation of the local sensory and sympathetic regulation on newly formed bone was investigated. The study found that H₂ supplantation increased the sensory CGRP expression in both neo-tissue surrounding the fracture gap and hard callus (Fig. 7A). Simultaneously, there is a significant decrease in the expression of adrenergic NE in neo-tissue at the fracture gap, TH (Fig. 7A) and adrenergic receptors ADRB1 and ADRB2 (Fig. 7B) in both neo-tissue near the fracture line and bony callus. These findings suggest that the enhanced bone regeneration observed with H₂ supplantation might be mediated by local sensory and sympathetic inhibition pathways.

When eliminating H₂ to observe other degradation products on the local sensory and sympathetic regulation. The data showed a significant increase in CGRP expression in the newly formed bone at the peripheral cortex compared to the control group (Fig. 7C). Additionally, the high expressions of adrenergic NE and TH in SS-IMN group were markedly suppressed by the degradation products (Fig. 7C). The inhibitory effects on these neurotransmitters were partially evident in Mg(OH)₂-IMN, MgCl₂-IMN, and NaOH-IMN, albeit to a lesser extent compared to Mg-IMN (Fig. 7C). Regarding adrenergic receptors, ADRB2 was notably downregulated in the newly formed bone at the peripheral cortex by Mg-IMN, followed by Mg(OH)₂-IMN and MgCl₂-IMN, but not affected by

NaOH-IMN (Fig. 7D). These findings indicate that degradation products of Mg activate local sensory nerves and concurrently inhibit sympathetic nerve modulation by reducing the neurotransmitters release to the local bone, particularly through ADRB2, at a weaker level than Mg-IMN, while alkaline pH alone did not affect adrenergic receptors.

4. Discussion

Mg-based implants have gained increasing attention for their great potential for enhancing bone regeneration via facilitating osteogenesis and angiogenesis [35–38]. Recent research mainly focused on the role of Mg²⁺ in bone regeneration. Yet the degradation of Mg not only resulted in increased Mg²⁺ but also generate H₂ and OH⁻, with the later generates a local alkaline environment. The interactions or effects of these three Mg degradation products on bone fracture repair however remain unclear. In the current study, we investigated the temporal-spatial degradation profiles of Mg implants in fractured osteoporotic femur, indicating Mg²⁺, H₂, and OH⁻ generated post Mg-IMN implantation mainly during the early stage of osteoporotic fracture healing. Moreover, we identified a previously undiscovered mechanism of sensory activation and sympathetic inhibition regulating Mg-IMN enhanced early stage of osteoporotic fracture healing, with comparable individual and synergistic contributions from Mg²⁺, H₂, and alkaline pH (Fig. 8). Mg-IMN, therefore, is of great potency to be applied for accelerating bone regeneration clinically.

4.1. The degradation profiles of biodegradable Mg implanted in fractured femur

One major contribution of our study is that we systemically detected Mg degradation *in vivo* and revealed the temporal-spatial degradation profiles of Mg-IMN implanted in the fractured osteoporotic femur. Upon implantation, Mg²⁺, H₂, and alkaline pH are generated according to the anodic and cathodic reaction $\text{Mg} + 2\text{H}_2\text{O} \rightarrow \text{Mg}^{2+} + 2\text{OH}^- + \text{H}_2$ [13,39]. The concentrations of degradation products at the implant interface are more important than the bulk value [40]. In this study, we observed the presence of H₂, an alkaline pH environment, and elevated Mg particularly around the implant interface within 15 days post-fracture. H₂ and alkaline pH values exhibited specific temporal patterns, showing dual peaks at 3 days and 9 days post-fracture *in vivo*. The first peak occurs on day 3, these degradation products could diffuse unhindered into the surrounding hematoma and bone marrow. As the second peak arises because of gradual tissue regeneration encircling the fracture gap, H₂ becomes increasingly saturated in the callus and bone marrow. Afterwards, Mg-IMN almost stops the degradation with only little H₂, and the alkaline pH return to neutral.

Previous studies have associated the rapid burst release of degradation products with concerns related to volume [41,42], our study observed a slow pit erosion pattern from the hole region of the IMN to the shielding region. Besides, the total Mg volume in this study being relatively small (approximately 10 mg for a 0.7 mm diameter, 1.5 cm length rod) with majority remained undegraded even at 6 and 12 weeks post-implantation, which is much smaller than Mg screws where Mg²⁺ concentration in plasma from bone marrow cavities around Mg screws *in vivo* only elevated from 0.95 mM to 1.07 mM within physical concentration (0.65–1.05 mM) after immersed for 72 hours [43], as the critical threshold without concerns of health risks of Mg concentration is 3.5 mM [44]. Furthermore, we found the peak H₂ concentration in bone marrow at 9 days was around 300 μM, much lower than the saturated H₂ concentration of 0.8 mM/1.6 ppm in liquid environments [45], and is insufficient to form gas bubble. Besides, no swelling, bleeding or gas pockets were observed at the fracture site during our experiments, partially attributed to the rapid diffusion and absorption capabilities of H₂, which is small molecular with high penetration potency [46], and no adverse effects on bone healing safety were observed as the gas was largely resorbed by the surrounding tissues [47,48]. The pH value at the

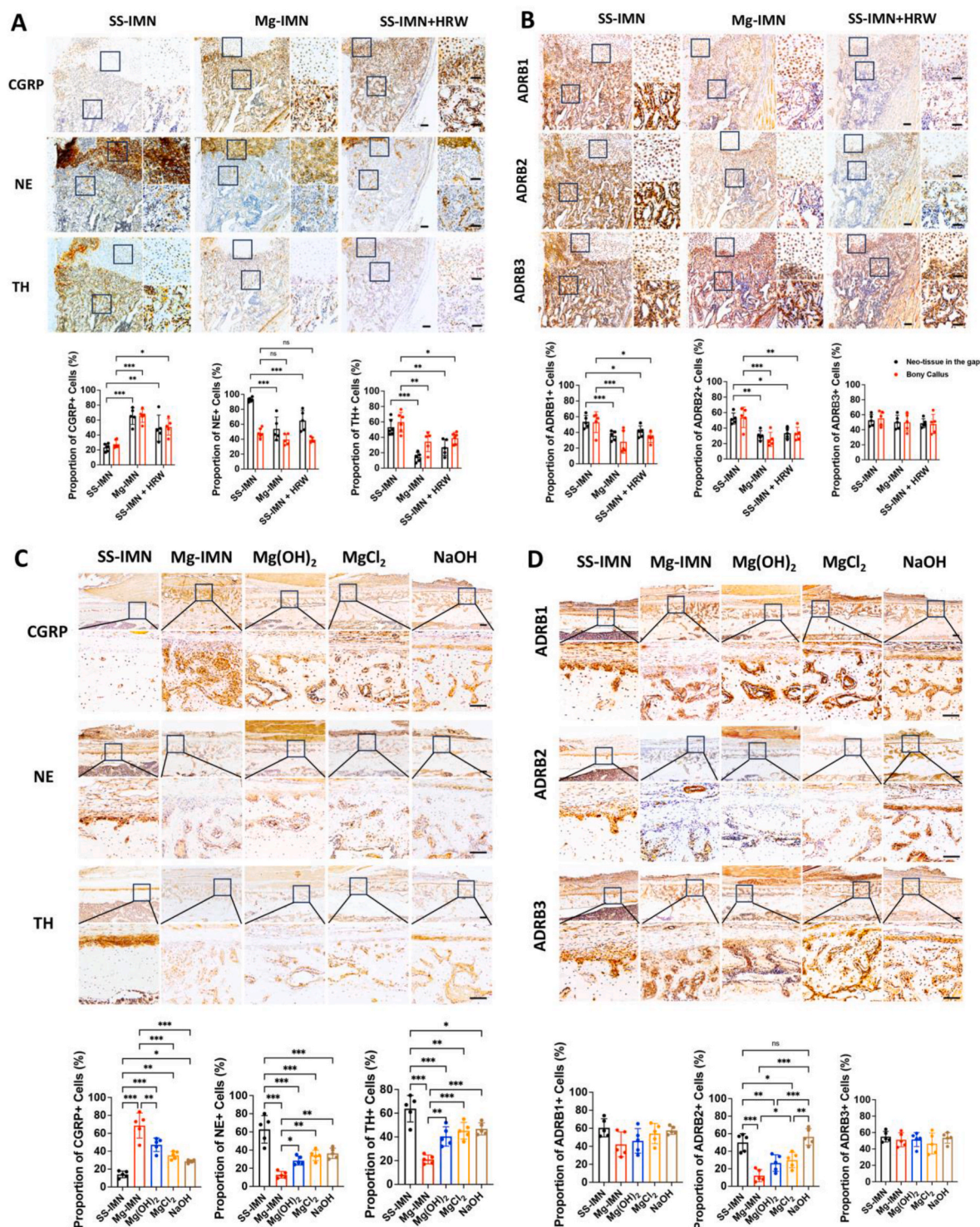


Fig. 7. Sensory and sympathetic regulation by the degradation products from Mg-IMN on bone regeneration. Immunohistochemical staining of CGRP, NE and TH (A), Adrenergic receptors (B) in osteoporotic fracture healing callus at 2 weeks of SS-IMN, Mg-IMN, and SS-IMN + HRW groups. Quantification (bellow) of the proportion of CGRP, NE, TH, ADRB1, ADRB2, and ADRB3 positive cells in neo-tissue and bony callus. $*p < 0.05$, $**p < 0.01$, $***p < 0.001$, ns, not significant, by one-way ANOVA with Tukey's *post hoc* test, $n = 5$ animals per group. Scale bars, 100 μm (main images), 50 μm (magnified images). Immunohistochemical staining of CGRP, NE and TH (C), Adrenergic receptors (D) in the newly formed bone at the peripheral cortex of rat femur implanted with SS-IMN, Mg-IMN, Mg(OH)₂-IMN, MgCl₂-IMN, NaOH-IMN in the distal femur for 2 weeks. Quantification (bellow) of proportion of CGRP, NE, TH, ADRB1, ADRB2, and ADRB3 positive cells in the newly formed bone at the peripheral cortex. $*p < 0.05$, $**p < 0.01$, $***p < 0.001$, ns, not significant, by one-way ANOVA with Tukey's *post hoc* test, $n = 5$ animals per group. Scale bars, 200 μm (main images), 50 μm (magnified images). Data throughout are presented as means \pm SD.

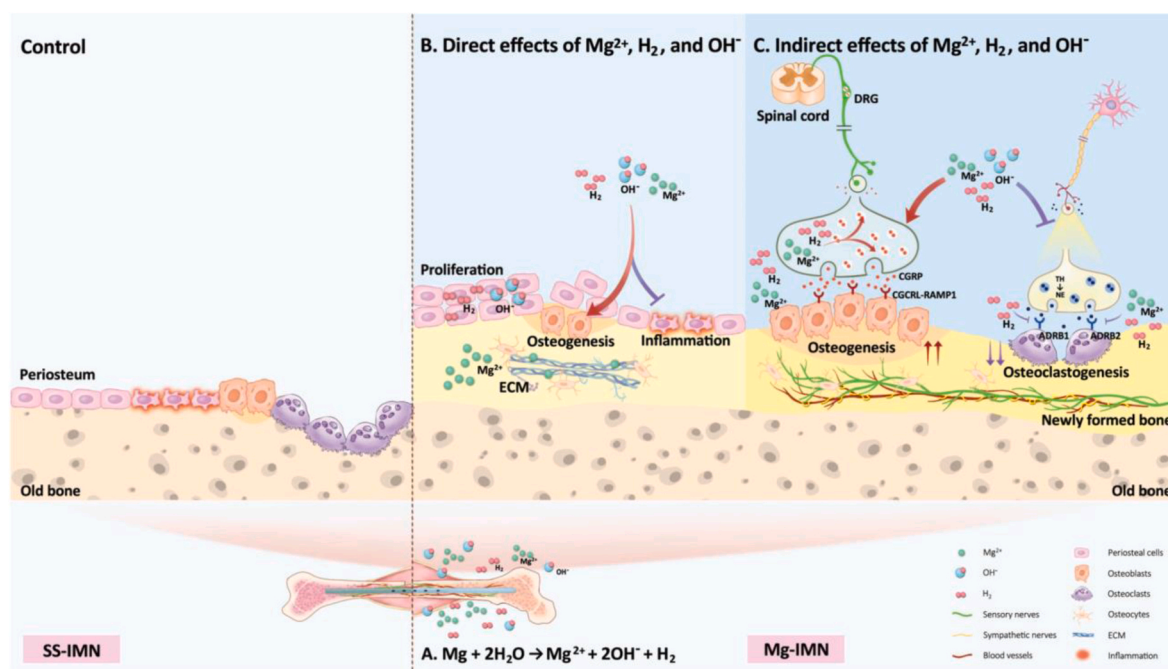


Fig. 8. Schematic diagram illustrating the distinct and synergistic effects of Mg^{2+} , H_2 , and OH^- released from biodegradable Mg on bone regeneration. (A) During the early osteoporotic fracture healing, the implantation of Mg-IMN releases Mg^{2+} , H_2 , and OH^- into tissues surrounding the fracture site. (B) The three degradation products directly enhance osteogenesis and reduce inflammation. Specifically, H_2 and OH^- (which create an alkaline pH environment) increase cell proliferation, while Mg^{2+} may primarily improve the extracellular matrix (ECM). (C) Mg^{2+} , H_2 , and OH^- contribute comparably to improved bone regeneration when implanted with Mg-IMN. This process involves the activation of sensory pathways and inhibition of sympathetic signaling. Notably, Mg^{2+} and H_2 , but not OH^- , increase the synthesis of CGRP and inhibit adrenergic receptors.

implant-bone interface is largely determined by the corrosion rate of Mg-containing implants, which tends to be alkaline, ranging from 8.0 to 8.5, while the bulk pH is close to the physiological pH maintained by acid-base balance in the body [40]. Consistent with this finding, our study showed that the pH value near the fracture line remained alkaline, ranging from 7.5 to 8.5 during the early osteoporotic fracture healing. Local alkalization triggers the precipitation of Ca^{2+} and PO_4^{3-} in body fluids, forming hydroxyapatite-like corrosion products and developed a protective layer on the metal surface [49], which may also be a reason for slowing down the degradation processes.

4.2. The individual and synergistic biological effects of three products generated from Mg metal *ex vivo* and *in vivo*

Another major finding is that the three Mg degradation products from Mg-IMN exert individual and synergistic biological effects on bone regeneration. Previous studies align with our findings that H_2 promotes autonomous stem cell early proliferation and tissue regeneration [33,50], enhances osteogenesis [51], and inhibits osteoclast differentiation [52]. ECM components, including collagen, are known to support stem cell migration and provide a scaffold for progenitor cells [53], and our RNA-seq data analysis well supports that Mg^{2+} upregulated genes involved in ECM-interaction and cell adhesion pathways. Furthermore, an alkaline pH environment may act as a trigger to stimulate regeneration and healing process to reestablish a functionalized environment [54], promote the synthesis and cross-linking of collagen, facilitate hydroxyapatite formation [55], induce osteoblast differentiation, and inhibit osteoclast activity [56,57]. These factors collectively contribute to creating a conducive microenvironment for bone healing and regeneration. Besides, the down-regulated DEGs by three degradation products significantly enriched in terms related to inhibition of inflammation, immunity, or apoptosis-related pathways. Our study reinforces the notion that Mg^{2+} is essential for inflammation and immune regulation [58–61]. In addition, H_2 exerts antioxidant, anti-apoptotic,

and anti-inflammatory activity on cell protection [33,62]. Consistent with the study that alkalization at pH 8.0–8.5 tends to be inhibitor of inflammasome activation, while acidification at pH 6.0–7.0 is a danger signal alerting innate immunity contributing to inflammation [63]. Overall, our study underscores the multiple roles of these Mg-IMN degradation products in bone healing and regeneration *ex vivo*.

The effects and contribution ratios of the three degradation products are further explored through *in vivo* studies. Our present study for the first time comprehensively revealed the effects and regulation on the early healing process post fracture by Mg-IMN, where the early stage is decisive for successful fracture healing [64]. Previous research focused on the Mg-IMN effects on osteoporotic fracture healing was investigated from 2 weeks to 12 weeks post-fracture onwards [10]. Our findings indicate Mg-IMN in the fractured femur mainly degraded during the initial 2 weeks after implantation. The early stage of fracture healing is characterized by conditions like low oxygen, low pH, and unbalanced Na^+ , K^+ ions levels [64], as H_2 can attenuate ROS levels in chronic intermittent hypoxia [65], alkaline pH environment and elevated Mg^{2+} occur during pure Mg degradation [13], and Mg^{2+} has been investigated for its capacity to enhance bone formation and osteogenesis [10,26]. Therefore, Mg implants increased bone regeneration, such a response, however, should not be solely ascribed to Mg^{2+} , a role of H_2 and alkaline environment should not be neglected. Our results showed mice treated with oral drinking H_2 -rich water (HRW) and intraperitoneal injection H_2 -rich saline (HRS), the commonly used methods of H_2 administration, making it the convenient option in clinical practice [33], significantly accelerated the osteoporotic fracture healing. In accordance with several other previous studies also reported the bone regeneration effects, H_2 contributes to the prevention of bone loss in osteoporosis through the ablation of oxidative stress [17], enhances zebrafish embryo osteogenesis [51], prevents osteoclast differentiation [52], and accelerates the fracture healing by attenuating autophagy [66]. Notably, in this study, intraperitoneal injection and oral drinking HRW generate not only affect local actions but also the systemic effects [33], after

eliminating the effect of H₂, both MgCl₂-IMN and NaOH-IMN implanted in rat distal femur formed substantially large amount of newly formed bone at the peripheral cortex, though the bone regeneration effects are less than that of Mg-IMN. Drinking alkaline water has been shown to improve spine BMD of postmenopausal women with osteoporosis [67], and Mg(OH)₂ enhances osteoblast activity and bone formation [68]. Our study confirms that the accelerated bone regeneration facilitated by Mg-IMN is attributed comparably to three degradation products: locally generated H₂, an alkaline pH environment, and elevated Mg²⁺. It is necessary to control equivalent doses of the degradation products from Mg-IMN for further studies to gain deeper insights into their effects on bone healing.

4.3. Sensory nerves activation by degradation products in bone regeneration

Bone regeneration is a complex process involving nerve-dependent mechanisms, the periosteum and trabecular bone compartments are densely innervated with sensory fibers extending from the DRG of the spinal cord, influencing bone metabolism and growth [34,69]. Mg-IMN significantly increased sensory CGRP expression in the callus during the early stage of fracture healing, in accordance with previous studies that Mg mental implantation accelerated bone regeneration with increased extracellular Mg²⁺, inducing elevated intracellular adenosine triphosphate (ATP) and CGRP vesicles aggregation in DRG [10,26]. Mg²⁺ has minimal effect on CGRP release of DRG in short-term *ex vivo* treatment without systemic nerve regulation, suggesting that Mg²⁺ requires intact sensory nerve pathways since previous research demonstrated increased Mg²⁺ influx notably enhanced CGRP release from the DRG *in vivo* [10]. The content of CGRP in the culture supernatant of rat DRG treated with HRM for 2 hours was increased by ELISA analysis. While HRW increased the sensory CGRP expression in both neo-tissues surrounding the fracture gap and hard callus *in vivo*, indicating that H₂ plays a crucial role in CGRP regulation, not only stimulate the release of CGRP from DRG, but also more CGRP binds to the local tissues to accelerate bone regeneration.

Separate administration of H₂, Mg²⁺, and alkaline pH significantly increased local sensory activity in the newly formed bone *in vivo*. Of interest, Mg²⁺ and H₂, but not alkaline pH alone, promoted the CGRP synthesis and vesicles accumulation in rat DRG *in vivo*. This aligns with the study showing that 10% MgCl₂ containing powder promoted bone formation via the skeleton interoceptive circuit, accompanied by sprouting and arborization of CGRP-positive nerve fibers in mice [26]. Limited research on skeletal interoceptive regulation effects of H₂ and alkaline pH has been conducted, however several studies indicated that H₂ exerts neuroprotective, anti-neuroinflammatory effects, alleviates neuropathic pain and neurological disorders mainly focusing on its antioxidant and anti-apoptotic properties [70–72]. Mg²⁺ stimulates local sensory fibers via Mg²⁺ transporters or channels (i.e., MAGT1 and TRPM7) [10,73]. Similarly, there might be specific transporters or channels for H₂ and alkaline-sensitive channels. The target especially of H₂ in human body remains relatively underexplored.

4.4. Sympathetic nerves suppression by degradation products in bone regeneration

Another novel finding from the present study is that we identify Mg-IMN and the degradation products enhanced bone regeneration possibly by concurrently suppressing sympathetic neuronal activity. Sympathetic tone is increased in sensory denervation models [74], the sympathetic NE and TH are catabolic factors [25,75]. It remains to be determined how sensory pathways mechanistically interact with sympathetic regulation, particularly when considering sensory neurons modulate bone regeneration by acting as a brake on the sympathetic nerves [76,77]. In our study, Mg-IMN significantly inhibited adrenergic NE and TH in newly formed tissues, a suppression that was partially observed with the

degradation products Mg²⁺, H₂, and alkaline pH. Mg²⁺ promotes new bone formation through prominent CGRP activity, and meanwhile suppresses sympathetic nerve [10,26], which conforms to our results. Recently, H₂ (inhalation 1.3 % H₂ + 21 % O₂ + 77.7 % N₂, 1 hour, daily) improved autonomic imbalance by suppressing the overactive sympathetic nervous system and augmenting the activity of the parasympathetic nervous system [78]. Additionally, extracellular acidification is a common feature in pain-generating pathological situations and extracellular H⁺ ions are regarded as a novel signal for TH activation [79], although direct evidence linking H₂, and alkaline pH to sympathetic regulation in bone regeneration is lacking.

NE released from sympathetic nerve terminals signals acts on α - and β -adrenergic receptors (ADRs) to regulate osteoblast and osteoclast activities [34,80,81], and global disruption of α -adrenoceptors barely affects bone tissue [82]. Our results confirmed that Mg-IMN suppressed both ADRB1 and ADRB2 in osteoporotic fracture callus. Mg²⁺ primarily targeted inhibition of ADRB2, in accordance with another study [26]. Exposure to H₂ led to an inhibitory expression of both ADRB1 and ADRB2. However, it seems alkaline pH alone has no direct effect on any ADRs and might indirectly suppress sympathetic transmitters, may because the different preferences for ADRs [83]. Overall, the accelerated bone regeneration facilitated by Mg-IMN and its degradation products appears to be mediated through the simultaneous suppression of sympathetic signaling, with the individual regulatory effects of the degradation products being less pronounced compared to Mg-IMN, reinforcing the notion that Mg-IMN offers a comprehensive approach to enhancing bone healing.

4.5. Limitations

This is a limitation when considering that the degradation of Mg in body liquid is complex, influenced by solution chemistry parameters, and interactions between metals and biomolecules. Precise control of degradation products and equivalent doses matching the degradation of Mg-IMN is crucial for accurately understanding their role, which is challenging to achieve during the bone healing process *in vivo*. It is also a limitation that the information conveyed by this study does not expand to time points beyond 2 weeks during the later stage of osteoporotic fracture healing. Further studies are required to address the unanswered question on the fate of Mg degradation in large animals or patients with diseased tissues, and to elucidate how neurotransmitters modulate the kinetics and magnitude of the combined host and Mg-IMN in nerve-bone interactions.

5. Conclusion

Taken together, the present study demonstrated that, upon Mg-IMN implantation in the fractured osteoporotic femur, the degradation profiles are systematically detected showing that Mg²⁺, H₂, and alkaline pH environment are generated mainly surrounding the fracture gap during the early healing phase within 15 days post-fracture. These factors individually and synergically promoted bone formation, with each contributing approximately one-third to the accelerated bone regeneration by Mg-IMN. We have identified the regulatory mechanism of sensory activation and simultaneously sympathetic suppression in Mg-IMN accelerated the early fracture healing process. This mechanism appears to be mediated by the generation of H₂, Mg²⁺, and an alkaline pH environment, collectively enhancing bone regeneration. The discovery of the three degradation products of Mg-IMN on bone regeneration through skeletal interception could consolidate our current understanding on the underlying mechanisms of Mg-IMN in the acceleration of bone regeneration and benefit its clinical application, such as one of our early clinical studies using biodegradable Mg screw for fixation of bony flap for effective treatment of osteonecrosis of femoral head (ONFH) as Mg ions, H₂ and alkaline pH environment are the three beneficial factors for targeting the underlying pathology of

corticosteroids induced ONFH [84].

CRediT authorship contribution statement

Yuanming An: Writing – review & editing, Writing – original draft, Visualization, Validation, Project administration, Methodology, Investigation, Formal analysis, Data curation, Conceptualization. **Haozhi Zhang:** Validation, Software, Methodology, Investigation, Formal analysis, Data curation. **Shi'an Zhang:** Validation, Software, Methodology, Formal analysis, Data curation. **Yuanta Zhang:** Validation, Software, Methodology, Data curation. **Lizhen Zheng:** Validation, Software, Methodology, Formal analysis. **Xin Chen:** Validation, Methodology. **Wenxue Tong:** Validation, Software, Resources, Methodology. **Jiankun Xu:** Writing – review & editing, Validation, Supervision, Resources, Project administration, Methodology, Funding acquisition, Data curation, Conceptualization. **Ling Qin:** Writing – review & editing, Visualization, Supervision, Resources, Project administration, Investigation, Funding acquisition, Conceptualization.

Data and materials availability

All data associated with this study are present in the paper and the Supplementary Materials. Additional data related to this paper may be requested from the authors.

Ethics approval and consent to participate

All animal experiment procedures performed in this study adhered to the principles for the care and use of laboratory animals approved by the Animal Experimentation Ethics Committee of the Chinese University of Hong Kong (Ref. No. 22/048/MIS-5-C and 22/092/MIS-5-C).

Funding

This work was supported by Areas of Excellence from the Research Grants Council of Hong Kong (AoE/M-402/20), and General Research Fund (14109421) from the Research Grants Council of Hong Kong.

Declaration of competing interests

The authors declare that they have no competing interests.

Appendix A. Supplementary data

Supplementary data to this article can be found online at <https://doi.org/10.1016/j.bioactmat.2024.12.020>.

References

- [1] G.B.D.F. Collaborators, Global, regional, and national burden of bone fractures in 204 countries and territories, 1990–2019: a systematic analysis from the Global Burden of Disease Study 2019, *Lancet Healthy Longev* 2 (9) (2021) e580–e592, [https://doi.org/10.1016/S2666-7568\(21\)00172-0](https://doi.org/10.1016/S2666-7568(21)00172-0).
- [2] T.K. Gill, M.M. Mittinty, L.M. March, J.D. Steinmetz, G.T. Culbreth, M. Cross, J.A. Kopec, A.D. Woolf, L.M. Haile, H. Hagins, Global, regional, and national burden of other musculoskeletal disorders, 1990–2020, and projections to 2050: a systematic analysis of the Global Burden of Disease Study 2021, *The Lancet Rheumatology* 5 (11) (2023) e670–e682.
- [3] V. Ponkilainen, I. Kuitunen, R. Liukkonen, M. Vaajala, A. Reito, M. Uimonen, The incidence of musculoskeletal injuries: a systematic review and meta-analysis, *Bone Joint Res* 11 (11) (2022) 814–825, <https://doi.org/10.1302/2046-3758.1111.BJR-2022-0181.R1>.
- [4] L. Wang, W. Yu, X. Yin, L. Cui, S. Tang, N. Jiang, L. Cui, N. Zhao, Q. Lin, L. Chen, H. Lin, X. Jin, Z. Dong, Z. Ren, Z. Hou, Y. Zhang, J. Zhong, S. Cai, Y. Liu, R. Meng, Y. Deng, X. Ding, J. Ma, Z. Xie, L. Shen, W. Wu, M. Zhang, Q. Ying, Y. Zeng, J. Dong, S.R. Cummings, Z. Li, W. Xia, Prevalence of osteoporosis and fracture in China: the China osteoporosis prevalence study, *JAMA Netw. Open* 4 (8) (2021) e2121106, <https://doi.org/10.1001/jamanetworkopen.2021.21106>.
- [5] M. Haseeb, M.F. Butt, T. Altaf, K. Muzaffar, A. Gupta, A. Jallu, Indications of implant removal: a study of 83 cases, *Int. J. Health Sci.* 11 (1) (2017) 1.
- [6] J.L. Wang, J.K. Xu, C. Hopkins, D.H. Chow, L. Qin, Biodegradable magnesium-based implants in orthopedics-A general review and perspectives, *Adv. Sci.* 7 (8) (2020) 1902443, <https://doi.org/10.1002/adv.201902443>.
- [7] L. Tian, Y. Sheng, L. Huang, D.H.-K. Chow, W.H. Chau, N. Tang, T. Ngai, C. Wu, J. Lu, L. Qin, An innovative Mg/Ti hybrid fixation system developed for fracture fixation and healing enhancement at load-bearing skeletal site, *Biomaterials* 180 (2018) 173–183.
- [8] D. Zhao, F. Witte, F. Lu, J. Wang, J. Li, L. Qin, Current status on clinical applications of magnesium-based orthopaedic implants: a review from clinical translational perspective, *Biomaterials* 112 (2017) 287–302.
- [9] M.N. Sarian, N. Iqbal, P. Sotoudehbagha, M. Razavi, Q.U. Ahmed, C. Sukotjo, H. Hermawan, Potential bioactive coating system for high-performance absorbable magnesium bone implants, *Bioact. Mater.* 12 (2022) 42–63.
- [10] Y. Zhang, J. Xu, Y.C. Ruan, M.K. Yu, M. O’Laughlin, H. Wise, D. Chen, L. Tian, D. Shi, J. Wang, Implant-derived magnesium induces local neuronal production of CGRP to improve bone-fracture healing in rats, *Nature medicine* 22 (10) (2016) 1160–1169.
- [11] N. Zheng, J. Xu, Y.C. Ruan, L. Chang, X. Wang, H. Yao, J. Wang, R. Zhang, Q. Xue, N. Tang, Magnesium facilitates the healing of atypical femoral fractures: a single-cell transcriptomic study, *Mater. Today* 52 (2022) 43–62.
- [12] Y. Li, J. Xu, J. Mi, X. He, Q. Pan, L. Zheng, H. Zu, Z. Chen, B. Dai, X. Li, Biodegradable magnesium combined with distraction osteogenesis synergistically stimulates bone tissue regeneration via CGRP-FAK-VEGF signaling axis, *Biomaterials* 275 (2021) 120984.
- [13] Y.F. Zheng, X.N. Gu, F. Witte, Biodegradable metals, *Mater. Sci. Eng. R Rep.* 77 (2014) 1–34.
- [14] M. Rondanelli, M.A. Faliva, A. Tartara, C. Gasparri, S. Perna, V. Infantino, A. Riva, G. Petrangolini, G. Peroni, An update on magnesium and bone health, *Biometals* 34 (4) (2021) 715–736, <https://doi.org/10.1007/s10534-021-00305-0>.
- [15] S. Castiglioni, A. Cazzaniga, W. Albisetti, J.A. Maier, Magnesium and osteoporosis: current state of knowledge and future research directions, *Nutrients* 5 (8) (2013) 3022–3033.
- [16] I. Ohsawa, M. Ishikawa, K. Takahashi, M. Watanabe, K. Nishimaki, K. Yamagata, K.-i. Katsura, Y. Katayama, S. Asoh, S. Ohta, Hydrogen acts as a therapeutic antioxidant by selectively reducing cytotoxic oxygen radicals, *Nature medicine* 13 (6) (2007) 688–694.
- [17] J.D. Guo, L. Li, Y.M. Shi, H.D. Wang, S.X. Hou, Hydrogen water consumption prevents osteopenia in ovariectomized rats, *Br. J. Pharmacol.* 168 (6) (2013) 1412–1420.
- [18] T.R. Arnett, Acid–base Regulation of Bone Metabolism, *International Congress Series*, Elsevier, 2007, pp. 255–267.
- [19] D.A. Bushinsky, Metabolic alkalosis decreases bone calcium efflux by suppressing osteoclasts and stimulating osteoblasts, *Am. J. Physiol. Ren. Physiol.* 271 (1) (1996) F216–F222.
- [20] J. Li, Z. Zhang, J. Tang, Z. Hou, L. Li, B. Li, Emerging roles of nerve–bone axis in modulating skeletal system, *Med. Res. Rev.* (2024).
- [21] R.E. Tomlinson, B.A. Christiansen, A.A. Giannone, D.C. Genetos, The role of nerves in skeletal development, adaptation, and aging, *Front. Endocrinol.* 11 (2020) 646, <https://doi.org/10.3389/fendo.2020.00646>.
- [22] P. Dimitri, C. Rosen, The central nervous system and bone metabolism: an evolving story, *Calcif. Tissue Int.* 100 (5) (2017) 476–485, <https://doi.org/10.1007/s00223-016-0179-6>.
- [23] J.M. Brazill, A.T. Beeve, C.S. Craft, J.J. Ivanusic, E.L. Scheller, Nerves in bone: evolving concepts in pain and anabolism, *J. Bone Miner. Res.* 34 (8) (2019) 1393–1406, <https://doi.org/10.1002/jbmr.3822>.
- [24] X. Chen, Magnesium-based implants: beyond fixators, *Journal of orthopaedic translation* 10 (2017) 1–4.
- [25] M. Zaidi, Skeletal remodeling in health and disease, *Nat Med* 13 (7) (2007) 791–801, <https://doi.org/10.1038/nm1593>.
- [26] W. Qiao, D. Pan, Y. Zheng, S. Wu, X. Liu, Z. Chen, M. Wan, S. Feng, K.M. Cheung, K. W. Yeung, Divalent metal cations stimulate skeleton interoception for new bone formation in mouse injury models, *Nat. Commun.* 13 (1) (2022) 535.
- [27] Y. Wang, V.H. Leung, Y. Zhang, V.S. Nudell, M. Loud, M.R. Servin-Vences, D. Yang, K. Wang, M.D. Moya-Garzon, V.L. Li, The role of somatosensory innervation of adipose tissues, *Nature* 609 (7927) (2022) 569–574.
- [28] S.M. de Smit, J.J. Langedijk, L.C. van Haalen, S.H. Lin, J.H. Bitter, D.P. Strik, Methodology for in situ microsensor profiling of hydrogen, pH, oxidation–reduction potential, and electric potential throughout three-dimensional porous cathodes of (bio) electrochemical systems, *Anal. Chem.* 95 (5) (2023) 2680–2689.
- [29] M. Jeyaraman, S. Muthu, P. Gangadharan, R. Ranjan, N. Jeyaraman, G.S. Prajwal, P. C. Mishra, R.L. Rajendran, B.C. Ahn, Osteogenic and chondrogenic potential of periosteum-derived mesenchymal stromal cells: do they hold the key to the future? *Pharmaceuticals* 14 (11) (2021) <https://doi.org/10.3390/ph14111133>.
- [30] M. Sobocki, K. Mrouj, J. Colinge, F. Gerbe, P. Jay, L. Krasinska, V. Dulic, D. Fisher, Cell-cycle regulation accounts for variability in Ki-67 expression levels, *Cancer Res.* 77 (10) (2017) 2722–2734.
- [31] T. Komori, Molecular mechanism of Runx2-dependent bone development, *Mol. Cell.* 43 (2) (2020) 168–175.
- [32] Y. Sun, L. Chen, S. Ma, J. Zhou, H. Zhang, J.Q. Feng, C. Qin, Roles of DMP1 processing in osteogenesis, dentinogenesis and chondrogenesis, *Cells Tissues Organs* 194 (2–4) (2011) 199–204.
- [33] M.Y. Artamonov, A.K. Martusevich, F.A. Pyatakovich, I.A. Minenko, S.V. Dlin, T. W. LeBaron, Molecular hydrogen: from molecular effects to stem cells management and tissue regeneration, *Antioxidants* 12 (3) (2023) 636.

- [34] W. Sun, B. Ye, S. Chen, L. Zeng, H. Lu, Y. Wan, Q. Gao, K. Chen, Y. Qu, B. Wu, Neuro-bone tissue engineering: emerging mechanisms, potential strategies, and current challenges, *Bone Research* 11 (1) (2023) 65.
- [35] Y. Luo, J. Wang, M.T.Y. Ong, P.S.-h. Yung, J. Wang, L. Qin, Update on the research and development of magnesium-based biodegradable implants and their clinical translation in orthopaedics, *Biomaterials Translational* 2 (3) (2021) 188.
- [36] Z. Shan, X. Xie, X. Wu, S. Zhuang, C. Zhang, Development of degradable magnesium-based metal implants and their function in promoting bone metabolism (A review), *Journal of Orthopaedic Translation* 36 (2022) 184–193.
- [37] Q. Zhang, Z. Chen, Y. Peng, Z. Jin, L. Qin, The novel magnesium–titanium hybrid cannulated screws for the treatment of vertical femoral neck fractures: biomechanical evaluation, *Journal of Orthopaedic Translation* 42 (2023) 127–136.
- [38] J. Espiritu, M. Meier, J.-M. Seitz, The current performance of biodegradable magnesium-based implants in magnetic resonance imaging: a review, *Bioact. Mater.* 6 (12) (2021) 4360–4367.
- [39] F. Witte, N. Hort, C. Vogt, S. Cohen, K.U. Kainer, R. Willumeit, F. Feyerabend, Degradable biomaterials based on magnesium corrosion, *Current opinion in solid state and materials science* 12 (5–6) (2008) 63–72.
- [40] A.S. Gnedenkov, D. Mei, S.V. Lamaka, S.L. Sinebryukhov, D.V. Mashtalyar, I. E. Vyalyi, M.L. Zheludkevich, S.V. Gnedenkov, Localized currents and pH distribution studied during corrosion of MA8 Mg alloy in the cell culture medium, *Corrosion Sci.* 170 (2020), <https://doi.org/10.1016/j.corsci.2020.108689>.
- [41] M. Nasr Azadani, A. Zahedi, O.K. Bowoto, B.I. Oladapo, A review of current challenges and prospects of magnesium and its alloy for bone implant applications, *Progress in Biomaterials* 11 (1) (2022) 1–26.
- [42] J. Dong, J. Zhong, R. Hou, X. Hu, Y. Chen, H. Weng, Z. Zhang, B. Liu, S. Yang, Z. Peng, Polymer bilayer-Micro arc oxidation surface coating on pure magnesium for bone implantation, *Journal of Orthopaedic Translation* 40 (2023) 27–36.
- [43] J. Wang, F. Witte, T. Xi, Y. Zheng, K. Yang, Y. Yang, D. Zhao, J. Meng, Y. Li, W. Li, Recommendation for modifying current cytotoxicity testing standards for biodegradable magnesium-based materials, *Acta Biomater.* 21 (2015) 237–249.
- [44] N.-E.L. Saris, E. Mervaa, H. Karpunen, J.A. Khawaja, A. Lewenstam, Magnesium: an update on physiological, clinical and analytical aspects, *Clinica chimica acta* 294 (1–2) (2000) 1–26.
- [45] G. Russell, A. Nenov, H. Kisher, J.T. Hancock, Molecular hydrogen as medicine: an assessment of administration methods, *Hydrogen* 2 (4) (2021) 444–460, <https://doi.org/10.3390/hydrogen2040025>.
- [46] T.W. LeBaron, I. Laher, B. Kura, J. Slezak, Hydrogen gas: from clinical medicine to an emerging ergogenic molecule for sports athletes, *Can. J. Physiol. Pharmacol.* 97 (9) (2019) 797–807.
- [47] K. Xie, L. Wang, Y. Guo, S. Zhao, Y. Yang, D. Dong, W. Ding, K. Dai, W. Gong, G. Yuan, Effectiveness and safety of biodegradable Mg–Nd–Zr alloy screws for the treatment of medial malleolar fractures, *Journal of Orthopaedic Translation* 27 (2021) 96–100.
- [48] T. Kraus, S.F. Fischerauer, A.C. Hänzli, P.J. Uggowitzer, J.F. Löffler, A.M. Weinberg, Magnesium alloys for temporary implants in osteosynthesis: in vivo studies of their degradation and interaction with bone, *Acta Biomater.* 8 (3) (2012) 1230–1238.
- [49] S. Amukarimi, M. Mozafari, Biodegradable magnesium-based biomaterials: an overview of challenges and opportunities, *MedComm* 2 (2) (2021) 123–144.
- [50] P. Zhao, Z. Dang, M. Liu, D. Guo, R. Luo, M. Zhang, F. Xie, X. Zhang, Y. Wang, S. Pan, X. Ma, Molecular hydrogen promotes wound healing by inducing early epidermal stem cell proliferation and extracellular matrix deposition, *Inflamm. Regen.* 43 (1) (2023) 22, <https://doi.org/10.1186/s41232-023-00271-9>.
- [51] M. Carnovali, M. Mariotti, G. Banfi, Molecular hydrogen enhances osteogenesis in Danio rerio embryos, *J. Fish. Biol.* 98 (5) (2021) 1471–1474.
- [52] D.-Z. Li, Q.-X. Zhang, X.-X. Dong, H.-D. Li, X. Ma, Treatment with hydrogen molecules prevents RANKL-induced osteoclast differentiation associated with inhibition of ROS formation and inactivation of MAPK, AKT and NF- κ B pathways in murine RAW264.7 cells, *J. Bone Miner. Metabol.* 32 (5) (2014) 494–504.
- [53] H. Zhou, B. Liang, H. Jiang, Z. Deng, K. Yu, Magnesium-based biomaterials as emerging agents for bone repair and regeneration: from mechanism to application, *J. Magnesium Alloys* 9 (3) (2021) 779–804, <https://doi.org/10.1016/j.jma.2021.03.004>.
- [54] Y. Shen, W. Liu, K. Lin, H. Pan, B.W. Darvell, S. Peng, C. Wen, L. Deng, W.W. Lu, J. Chang, Interfacial pH: a critical factor for osteoporotic bone regeneration, *Langmuir* 27 (6) (2011) 2701–2708, <https://doi.org/10.1021/la104876w>.
- [55] H. Peng, K. Fan, R. Zan, Z.-J. Gong, W. Sun, Y. Sun, W. Wang, H. Jiang, J. Ni, T. Suo, Degradable magnesium implants inhibit gallbladder cancer, *Acta Biomater.* 128 (2021) 514–522.
- [56] H. Wu, Y. Yin, X. Hu, C. Peng, Y. Liu, Q. Li, W. Huang, Q. Huang, Effects of environmental pH on macrophage polarization and osteoimmunomodulation, *ACS Biomater. Sci. Eng.* 5 (10) (2019) 5548–5557, <https://doi.org/10.1021/acsbomaterials.9b01181>.
- [57] R. Fliebel, C. Popov, M. Troltsch, J. Kuhnisch, M. Ehrenfeld, S. Otto, Mesenchymal stem cell proliferation and mineralization but not osteogenic differentiation are strongly affected by extracellular pH, *J. Cranio-Maxillo-Fac. Surg.* 44 (6) (2016) 715–724, <https://doi.org/10.1016/j.jcms.2016.03.003>.
- [58] S. Ashique, S. Kumar, A. Hussain, N. Mishra, A. Garg, B.J. Gowda, A. Farid, G. Gupta, K. Dua, F. Taghizadeh-Hesary, A narrative review on the role of magnesium in immune regulation, inflammation, infectious diseases, and cancer, *J. Health Popul. Nutr.* 42 (1) (2023) 74.
- [59] K. Xie, N. Wang, Y. Guo, S. Zhao, J. Tan, L. Wang, G. Li, J. Wu, Y. Yang, W. Xu, Additively manufactured biodegradable porous magnesium implants for elimination of implant-related infections: an in vitro and in vivo study, *Bioact. Mater.* 8 (2022) 140–152.
- [60] R. Ma, Y.-x. Lai, L. Li, H.-l. Tan, J.-l. Wang, Y. Li, T.-t. Tang, L. Qin, Bacterial inhibition potential of 3D rapid-prototyped magnesium-based porous composite scaffolds—an in vitro efficacy study, *Sci. Rep.* 5 (1) (2015) 13775.
- [61] B. Li, P. Thebaud, B. Labat, G. Ladam, V. Alt, M. Rupp, C. Brochhausen, J. Jantsch, M. Ip, N. Zhang, Implants coating strategies for antibacterial treatment in fracture and defect models: a systematic review of animal studies, *Journal of Orthopaedic Translation* 45 (2024) 24–35.
- [62] J. Slezak, B. Kura, T.W. LeBaron, P.K. Singal, J. Buday, M. Barancik, Oxidative stress and pathways of molecular hydrogen effects in medicine, *Curr. Pharmaceut. Des.* 27 (5) (2021) 610–625.
- [63] K. Rajamäki, T. Nordström, K. Nurmi, K.E. Åkerman, P.T. Kovanen, K. Öörni, K. K. Eklund, Extracellular acidosis is a novel danger signal alerting innate immunity via the NLRP3 inflammasome, *J. Biol. Chem.* 288 (19) (2013) 13410–13419, <https://doi.org/10.1074/jbc.M112.426254>.
- [64] G.N. Duda, S. Geissler, S. Checa, S. Tzitsionis, A. Petersen, K. Schmidt-Bleek, The decisive early phase of bone regeneration, *Nat. Rev. Rheumatol.* (2023) 1–18.
- [65] J. Song, Q. Chen, S. Xu, Y. Gou, Y. Guo, C. Jia, C. Zhao, Z. Zhang, B. Li, Y. Zhao, Hydrogen attenuates chronic intermittent hypoxia-induced cardiac hypertrophy by regulating iron metabolism, *Curr. Issues Mol. Biol.* 45 (12) (2023) 10193–10210.
- [66] J. Guo, S. Tian, Z. Wang, Y. Wang, X. Zhang, Y. Zhang, Z. Hou, W. Dong, Hydrogen saline water accelerates fracture healing by suppressing autophagy in ovariectomized rats, *Front. Endocrinol.* 13 (2022) 962303, <https://doi.org/10.3389/fendo.2022.962303>.
- [67] S. Fasihi, S. Fazelian, F. Farahbod, F. Moradi, M. Dehghan, Effect of alkaline drinking water on bone density of postmenopausal women with osteoporosis, *J. Menopausal Med* 27 (2) (2021) 94–101, <https://doi.org/10.6118/jmm.20036>.
- [68] C. Janning, E. Willbold, C. Vogt, J. Nellesen, A. Meyer-Lindenberg, H. Windhagen, F. Thorey, F. Witte, Magnesium hydroxide temporarily enhancing osteoblast activity and decreasing the osteoclast number in peri-implant bone remodelling, *Acta Biomater.* 6 (5) (2010) 1861–1868, <https://doi.org/10.1016/j.actbio.2009.12.037>.
- [69] F. Eleftheriou, Impact of the autonomic nervous system on the skeleton, *Physiol. Rev.* 98 (3) (2018) 1083–1112.
- [70] Y. Wang, P. Wang, C. Liu, W. Chen, P. Wang, L. Jiang, Hydrogen-rich saline attenuates chronic allodynia after bone fractures via reducing spinal CXCL1/CXCR2-mediated iron accumulation in mice, *Brain Sci.* 12 (12) (2022), <https://doi.org/10.3390/brainsci12121610>.
- [71] N. Lian, M. Shen, K. Zhang, J. Pan, Y. Jiang, Y. Yu, Y. Yu, Drinking hydrogen-rich water alleviates chemotherapy-induced neuropathic pain through the regulation of gut microbiota, *J. Pain Res.* (2021) 681–691.
- [72] M. Martínez-Serrat, I. Martínez-Martel, S. Coral-Pérez, X. Bai, G. Batallé, O. Pol, Hydrogen-rich water as a novel therapeutic strategy for the affective disorders linked with chronic neuropathic pain in mice, *Antioxidants* 11 (9) (2022), <https://doi.org/10.3390/antiox11091826>.
- [73] W. Qiao, K.H. Wong, J. Shen, W. Wang, J. Wu, J. Li, Z. Lin, Z. Chen, J. P. Matinlinna, Y. Zheng, TRPM7 kinase-mediated immunomodulation in macrophage plays a central role in magnesium ion-induced bone regeneration, *Nat. Commun.* 12 (1) (2021) 2885.
- [74] B. Hu, X. Lv, H. Chen, P. Xue, B. Gao, X. Wang, G. Zhen, J.L. Crane, D. Pan, S. Liu, Sensory nerves regulate mesenchymal stromal cell lineage commitment by tuning sympathetic tones, *J. Clin. Investig.* 130 (7) (2020) 3483–3498.
- [75] J. Xu, J. Wang, X. Chen, Y. Li, J. Mi, L. Qin, The effects of calcitonin gene-related peptide on bone homeostasis and regeneration, *Curr. Osteoporos. Rep.* 18 (6) (2020) 621–632, <https://doi.org/10.1007/s11914-020-00624-0>.
- [76] J. Xu, Z. Zhang, J. Zhao, C.A. Meyers, S. Lee, Q. Qin, A.W. James, Interaction between the nervous and skeletal systems, *Front. Cell Dev. Biol.* 10 (2022) 976736.
- [77] G. Karsenty, S. Khosla, The crosstalk between bone remodeling and energy metabolism: a translational perspective, *Cell Metab* 34 (6) (2022) 805–817, <https://doi.org/10.1016/j.cmet.2022.04.010>.
- [78] K. Sugai, T. Tamura, M. Sano, S. Uemura, M. Fujisawa, Y. Katsumata, J. Endo, J. Yoshizawa, K. Homma, M. Suzuki, E. Kobayashi, J. Sasaki, Y. Hakamata, Daily inhalation of hydrogen gas has a blood pressure-lowering effect in a rat model of hypertension, *Sci. Rep.* 10 (1) (2020) 20173, <https://doi.org/10.1038/s41598-020-77349-8>.
- [79] V.Q. Le, M. Eldani, M. Truong, K. Wimalasena, Extracellular H⁺ ions are a novel signal for tyrosine hydroxylase activation in catecholaminergic cells, *ACS Chem. Neurosci.* 14 (10) (2023) 1774–1784.
- [80] Y. Xiao, C. Han, Y. Wang, X. Zhang, R. Bao, Y. Li, H. Chen, B. Hu, S. Liu, Interceptive regulation of skeletal tissue homeostasis and repair, *Bone Res* 11 (1) (2023) 48, <https://doi.org/10.1038/s41413-023-00285-6>.
- [81] M. Maryanovich, S. Takeishi, P.S. Frenette, Neural regulation of bone and bone marrow, *Cold Spring Harb Perspect Med* 8 (9) (2018), <https://doi.org/10.1101/cshperspect.a031344>.
- [82] G.M. Martins, M. Teixeira, M.V. Silva, B. Neofiti-Papi, M. Miranda-Rodrigues, P. C. Brum, C.H.A. Gouveia, Global disruption of α 2A adrenoceptor barely affects bone tissue but minimizes the detrimental effects of thyrotoxicosis on cortical bone, *Front. Endocrinol.* 9 (2018) 486, <https://doi.org/10.3389/fendo.2018.00486>.
- [83] R. Tao, B. Mi, Y. Hu, S. Lin, Y. Xiong, X. Lu, A.C. Panayi, G. Li, G. Liu, Hallmarks of peripheral nerve function in bone regeneration, *Bone Res* 11 (1) (2023) 6, <https://doi.org/10.1038/s41413-022-00240-x>.
- [84] D. Zhao, S. Huang, F. Lu, B. Wang, L. Yang, L. Qin, K. Yang, Y. Li, W. Li, W. Wang, Vascularized bone grafting fixed by biodegradable magnesium screw for treating osteonecrosis of the femoral head, *Biomaterials* 81 (2016) 84–92.